Male-Biased Cyp17a2 Governs Antiviral Sexual Dimorphism in Fish via STING Stabilization and Viral Protein Degradation

Long-Feng Lu[a,c,1], Bao-jie Cui[a,e,1], Sheng-Chi Shi[a,c,1], Yang-Yang Wang[a,c], Can Zhang[a,c], Xiao Xu[a,e], Meng-Ze Tian[a,c], Zhen-Qi Li[a,c], Na Xu[a,c], Zhuo-Cong Li[a,c], Dan-Dan Chen[a,c], Li Zhou[a,c], Gang Zhai[a,c,2], Zhan Yin[f,a,c,2], Shun Li[a,b,c,d,e,2]

[a]Key Laboratory of Breeding Biotechnology and Sustainable Aquaculture, Institute of Hydrobiology, Chinese Academy of Sciences, Wuhan, Hubei 430072, China

[b]Laboratory for Marine Biology and Biotechnology, Qingdao Marine Science and Technology Center

[c]University of Chinese Academy of Sciences, Beijing, China

[d]Key Laboratory of Aquaculture Disease Control, Ministry of Agriculture, Wuhan, China

[e]College of Fisheries and Life Science, Dalian Ocean University, Dalian, China

[f]Key Laboratory of Mariculture, Ministry of Education, Ocean University of China, Qingdao 266003, China

[1]These authors have contributed equally to this work

[2]To whom correspondence may be addressed. Email: bob@ihb.ac.cn, zyin@ihb.ac.cn and zhaigang@ihb.ac.cn

Abstract

Differences in immunity between males and females in living organisms are generally thought to be due to sex hormones and sex chromosomes, and it is often assumed that males have a weaker immune response. Here we report that in fish, males exhibit stronger antiviral immune responses, which are driven by the male-biased gene Cyp17a2 rather than by hormones or sex chromosomes. First, we observed that male zebrafish exhibit enhanced antiviral resistance compared to females, and notably, zebrafish lack sex chromosomes. Through transcriptomic screening, we found that *cyp17a2* was specifically highly expressed in male fish. *Cyp17a2* knockout males were equivalent to wild-type males in terms of sex organs and androgen secretion, but the ability to upregulate IFN as well as antiviral resistance was greatly reduced. Then, Cyp17a2 is identified as a positive IFN regulator which located at endoplasmic reticulum, and specifically interacts with and enhances STING mediated antiviral responses. Mechanistically, Cyp17a2 stabiles STING expression by recruiting the E3 ubiquitin ligase TRIM11, which facilitates K33-linked polyubiquitination. The capacity of IFN induction of Cyp17a2 was abolished when STING is knockdown. Meanwhile, Cyp17a2 also attenuates viral infection directly to strengthen the antiviral capacity as an antiviral protein, Cyp17a2 degrades the spring viremia of carp virus (SVCV) P protein by utilizing USP8 to reduce its K33-linked polyubiquitination. These findings reveal a sex-based regulatory mechanism in teleost antiviral immunity, broadening our understanding of sexual dimorphism in immune responses beyond the conventional roles of sex chromosomes and hormones.

Keywords

Cyp17a2; Sexual Dimorphism; STING; SVCV; Ubiquitination

Introduction

Research has demonstrated that innate immune responses to viruses differ significantly between the sexes. Males exhibit heightened susceptibility to viral pathogens, correlating with their generally weaker innate immune activation compared to females[1]. This immunological dimorphism manifests clinically as elevated infection intensity (quantified by intra-host viral load) and prevalence (population-level infection rates) in males[2]. Notably, sex-specific clinical outcomes are exemplified by severe acute respiratory syndrome coronavirus 2 (SARS-CoV-2) infections, where epidemiological data suggest males face twice the risk of intensive care unit (ICU) admission and a 30% higher mortality rate compared to females[3]. Similar trends extend to other viral pathogens including Dengue virus, hantaviruses, and hepatitis B/C viruses, all exhibiting male-biased infection prevalence[4].

Several factors have been identified as contributors to these sex-specific disparities in antiviral immunity, including hormonal variations and sex chromosomes. For instance, androgens such as testosterone exhibit broad immunosuppressive effects, including reduced NK cell cytotoxicity, impaired neutrophil chemotaxis, and attenuated macrophage proinflammatory cytokine production *in vitro*[5]. In addition, the Y chromosome harbors only two annotated miRNAs, while the X chromosome contains numerous immune-relevant miRNAs, and emerging evidence implicates X-escapee miRNAs as key modulators of sex-biased immune responses[6].

It is well known that the interferon (IFN) response is an important host immune response to viral infection, in both mammals and fish[7]. The signaling pathways that activate IFN expression, although slightly different in fish and mammals, are generally conserved in both[8]. The endoplasmic reticulum (ER) protein stimulator of IFN genes (STING) is an important antiviral protein capable of resisting both DNA and RNA viruses by activating TANK binding kinase 1 (TBK1) during the induction of IFN production, which in turn phosphorylates IFN regulatory Factor 3 (IRF3) in the nucleus and activates the signaling of IFN transcription[9]. For instance, STING deficiency has been shown to impair innate immune responses against multiple RNA

viruses, such as dengue virus, West Nile virus, and Japanese encephalitis virus[10]. Notably, oncogenes of the DNA tumor viruses, including human papillomavirus E7 and adenovirus E1A, function as potent and specific inhibitors of the cyclic GMP-AMP synthase (cGAS)-STING signaling pathway[11].

Cyp17a is classified within the cytochrome P450 (CYP450) family. In mammals, there is only one form, cyp17a1, which possesses both hydroxylase and lyase functions. Mutations in the human *cyp17a1* gene are associated with congenital adrenal hyperplasia (CAH)[12]. Comparative genomic analyses reveal that teleost fishes possess two distinct *cyp17a* isoforms, the evolutionarily conserved *cyp17a1* and a phylogenetically divergent *cyp17a2* paralog, with the latter representing a teleost-specific innovation absent in mammalian genomes[13]. Current investigations of Cyp17a2 in teleost species have predominantly centered on its mechanistic roles governing sexual development and differentiation, for example, with knockout of zebrafish *cyp17a2* leads to significant impairment of sperm motility[14]. Although Cyp17a2 has been characterized in sexual development, its non-canonical physiological roles have yet to be fully elucidated.

In most vertebrates, the XY sex chromosomes exhibit significant physiological differences between males and females, as exemplified in humans. However, the sex determination mechanisms in fish are more complex. For instance, zebrafish lack sex chromosomes, which confers a natural advantage. This absence allows for the exclusion of sex chromosome-related differences in the study of immunological disparities between males and females. Consequently, we selected zebrafish as the model organism for this investigation. This enabled us to more precisely identify the genes that are differentially expressed in male and female autosomes, which is crucial for understanding the immunological differences between the sexes. This study elucidates the role of the teleost-specific gene *cyp17a2* in antiviral immunity, providing new insights into the evolutionary adaptation of immune systems and expanding our understanding beyond the traditional roles of sex chromosomes and hormones.

Results

1. Male fish exhibit enhanced resistance to viral infection compared to female fish

To determine whether sex differences exist in the antiviral response capacity of fish, age-matched female and male zebrafish were intraperitoneally (i.p.) injected with SVCV. Male fish exhibited a significantly higher survival rate than female fish within seven days post-infection (Fig. 1A). Concurrently, females demonstrated a markedly higher incidence of cutaneous hemorrhages relative to males (Fig. 1B). Consistent with the reduced mortality, male fish showed less tissue damage in the liver and spleen following viral infection (Fig. 1C). IF analysis revealed that the SVCV N protein, represented by green fluorescence, was barely detectable in male tissues but was prominently present in female tissues (Fig. 1D). At the mRNA level, viral transcripts were quantified in these tissues, and the abundance of *svcv-n* gene was significantly lower in male tissues (Fig. 1E). At the protein level, SVCV N and G proteins were less frequently detected in male tissues compared to female tissues in 7 samples (Fig. 1F). Additionally, viral titers were significantly lower in the hearts of male fish compared to female fish (Fig. 1G). These findings demonstrate a stronger antiviral response capacity in male fish compared to female fish.

2. Male-biased gene cyp17a2 orchestrates antiviral immunity through RLR pathway

To explore the potential causes of the observed differences in virus resistance between male and female fish, transcriptome sequencing was performed on head-kidney tissues of healthy hermaphroditic adult zebrafish. A total of 1,709 differentially expressed genes were identified (Fig. 2A and 2B). Among these, *cyp17a2* exhibits male-biased upregulation as a sex-related gene, and it was confirmed by subsequent qPCR (Fig. 2C and 2D). Furthermore, we systematically quantified Cyp17a2 mRNA and protein expression in multiple tissues of male and

female zebrafish, demonstrating a consistent male-biased expression pattern of Cyp17a2 (Fig. 2E and 2F). Thus, Cyp17a2 was selected for further study. We first sought to understand whether it was associated with host antiviral immunity, and the significant upregulation of the Cyp17a2 at the mRNA and protein level in response to viral stimulation suggested its possible involvement in the antiviral process (Fig. 2G and 2H). Following generation of *cyp17a2* knockout zebrafish, previous study revealed that male *cyp17a2*$^{-/-}$ mutants displayed normal development of male-typical secondary sexual characteristics comparable to WT males. However, female *cyp17a2*$^{-/-}$ mutants exhibited significantly underdeveloped genital papillae compared to their WT counterparts. To eliminate potential confounding effects of androgen-mediated pathways on immune parameters, subsequent experiments were conducted exclusively using male specimens from both genotypes. The male *cyp17a2*$^{-/-}$ mutants exhibited a higher mortality rate than WT males after viral infection (Fig. 2I). Significant tissue damage and strong green fluorescence representing the SVCV N protein was observed in the *cyp17a2*$^{-/-}$ tissues, virus titers assay also confirmed that viral proliferation was higher in *cyp17a2*$^{-/-}$ group (Fig. 2J-2L). Consistent with these observations, the replication of viral genes transcription and protein levels were increased in *cyp17a2*$^{-/-}$ homozygote tissues, these data demonstrated that Cyp17a2 is crucial for host antiviral defense (Fig. 2M and 2N). To further understand their functional mechanisms, a transcriptomic analysis contains total of 3,114 differentially expressed genes (DEGs) were identified, there are 1,217 genes upregulated and 1,897 were downregulated in the liver of *cyp17a2* knockout male zebrafish compared to WT males after viral infection (Fig. S1). Kyoto encyclopedia of genes and genomes (KEGG) pathway analysis revealed RIG-I-like receptors (RLRs), NOD-like receptors (NLRs), and Toll-like receptors (TLRs) signaling pathways were significantly affected (Fig. 2O). Gene set enrichment analysis (GSEA) showed that RLRs were downregulated in *cyp17a2*$^{-/-}$ group under SVCV infection, combining with numerous IFN-stimulated genes decreasing (ISGs) (Fig. 2P and Fig. S2). To validate the transcriptome data, *ifnφ1* levels were assessed and identified significantly downregulated in the *cyp17a2*$^{-/-}$ group (Fig. 2Q).

Collectively, these data suggest that viral proliferation was enhanced and IFN response were reduced in *cyp17a2*$^{-/-}$ fish.

3. Cyp17a2 enhances IFN expression and suppresses viral proliferation

Given the critical role of the IFN response in host defense against viral infections, we investigated the impact of Cyp17a2 on IFN expression and viral infection *in vitro*. Overexpression of Cyp17a2 significantly upregulated the IFN promoter and ISRE activities in response to poly I:C or SVCV stimulation (Fig. 3A-3C). An effective sh-*cyp17a2*#2 was generated and confirmed at both the mRNA and protein levels, and knockdown of *cyp17a2* inhibited both the IFN promoter and ISRE activity (Fig. 3D-3G). RNA sequencing analysis of the cell line revealed that SVCV infection activated IFN pathways in Cyp17a2-overexpressing cells, whereas these pathways were significantly suppressed upon *cyp17a2* knockdown (Fig. 3H). The induction or attenuation of IFN and ISGs upon Cyp17a2 overexpression or knockdown were confirmed by qPCR analysis, respectively (Fig. 3I). For antiviral capacity assays, Cyp17a2 from zebrafish and gibel carp both inhibited the proliferation of host-specific viruses, conversely, *cyp17a2* knockdown significantly enhanced viral proliferation (Fig. 3J and 3K). Regarding viral mRNA and proteins, overexpression or knockdown Cyp17a2 also displayed the similar opposite findings (Fig. 3L and 3M). IF assays indicated a lower intensity of green signals representing the viral protein in the Cyp17a2 overexpression group compared to the control, while a higher green signal was observed in the *cyp17a2* knockdown group relative to the normal group (Fig. 3N and 3O). These results suggest that Cyp17a2 upregulates IFN expression and enhances antiviral capacity in the host.

4. Cyp17a2 interacts with STING and stabilizes its expression

Given the critical role of the RLR signaling pathway in fish IFN activation, the relationship between Cyp17a2 and RLR signaling adaptors was investigated. Co-transfection with Myc-Cyp17a2 and Flag-tagged RLR components (MAVS, TBK1, STING, IRF3, IRF7) followed by anti-Flag immunoprecipitation identified specific

Cyp17a2-STING interaction via anti-Myc detection (Fig. 4A). Reciprocal Co-IP and semi-endogenous IP assays confirmed this interaction (Fig. 4B and 4C). Truncated STING mutants were generated to map binding domains (Fig. 4D). The transmembrane domain (TM)-deficient STING-ΔTM-HA failed to bind Cyp17a2, indicating TM domain dependence (Fig. 4E). Cyp17a2-GFP overlapped with ER markers in confocal microscopy and colocalized with STING but failed to colocalize with the ΔTM mutant (Fig. 4F and 4G). To identify the effect of Cyp17a2 on STING regulation, the mRNA level of *sting* was first analyzed, minimal change was observed in *sting* upon Cyp17a2 overexpression (Fig. 4H). Protein-level studies demonstrated Cyp17a2 remarkably enhanced STING abundance and confirmed by confocal microscopy (Fig. 4I and 4J). Endogenous STING was similarly stabilized dependent on Cyp17a2 under untreated or stimulated conditions (Fig. 4K). CHX chase assay showed prolonged exogenous and endogenous STING half-life with Cyp17a2 co-expression, and it was also confirmed by knockdown experiments (Fig. 4L-4N). These data demonstrate that Cyp17a2 binds STING via its TM and enhances STING posttranslational stability.

5. Cyp17a2 enhances STING-mediated IFN expression and antiviral responses

Considering that Cyp17a2 targets STING, a positive regulator of IFN production, we investigated whether Cyp17a2 influences the IFN expression induced by STING. The IFNφ1pro activity induced by STING overexpression was significantly enhanced by Cyp17a2, with similar amplification observed for ISRE promoter activation (Fig. 5A and 5B). Conversely, *cyp17a2* knockdown was shown to impair STING-mediated IFNφ1pro and ISRE activation (Fig. 5C and 5D). Corresponding increases in *ifn* and *vig1* transcripts were detected in Cyp17a2 overexpressing cells, while Cyp17a2 knockdown suppressed these responses (Fig. 5E and 5F). The subsequent investigation focused on the potential modulatory effect of Cyp17a2 on the STING-induced cellular antiviral response. STING overexpression reduced CPE, with viral titers decreased 336-fold compared to the control group. This protection was augmented by Cyp17a2 co-expression, achieving an additional 20-fold reduction (Fig. 5G and 5H). SVCV gene transcripts were suppressed by STING, with enhanced inhibition upon Cyp17a2 co-expression (Fig. 5I). IB and IF analysis

confirmed that Cyp17a2 potentiated STING-mediated suppression of viral protein expression (Fig. 5J and 5K). STING dependency was validated using shRNA knockdown (Fig. 5L). The antiviral capacity enhanced by Cyp17a2 was markedly attenuated in cells with *sting* knockdown, as evidenced by restored viral titers, gene and protein expression (Fig. 5M-5Q). These results demonstrate that Cyp17a2 potentiates STING activity to enhance IFN production and antiviral responses.

6. Cyp17a2 stabilizes STING through TRIM11-mediated K33-linked polyubiquitination

To elucidate the molecular mechanism by which Cyp17a2 augments STING stabilization, proteasomal and lysosomal degradation were pharmacologically inhibited using MG132 and CQ, respectively. Accelerated STING degradation caused by *cyp17a2* knockdown was rescued by MG132 but not CQ, suggesting knockdown of *cyp17a2* promoted STING degradation via the proteasome pathway (Fig. 6A). Then, enhanced polyubiquitination of STING was detected upon Cyp17a2 co-expression (Fig. 6B). Ubiquitin linkage analysis revealed selective enhancement of K33-linked chains, with *cyp17a2* knockdown shown to reduce both WT and K33-specific ubiquitination (Fig. 6C and 6D). Subsequently, candidate E3 ligases were screened, revealing TRIM11 and SOCS3a as STING interactors (Fig. 6E). TRIM11 was specifically identified as a Cyp17a2 binding partner through reciprocal Co-IP (Fig. 6F and 6G). Then the subcellular localization of TRIM11 was monitored, TRIM11-GFP signal overlapped with the red signals of the ER marker, indicating that TRIM11 colocalizes with the ER (Fig. 6H). Since the results identify that both STING and Cyp17a2 are localized to the ER, TRIM11 was examined for cellular localization with both STING and Cyp17a2, and the anticipated colocalization pattern was confirmed (Fig. 6I). Cyp17a2 was found to strengthen TRIM11-STING interaction (Fig. 6J). Functional assays demonstrated that TRIM11 augmented of Cyp17a2-mediated IFNφ1pro activity and *vig1* mRNA induction (Fig. 6K and 6L). TRIM11 potentiated the Cyp17a2-dependent stabilization of STING in both endogenous and exogenous systems (Fig. 6M). Two shRNAs target TRIM11 were

designed and generated, and after validating the knockdown efficiencies for both endogenous and exogenous targets, sh-*trim11*#2 was selected for the subsequent assay (Fig. 6N). The knockdown of TRIM11 impaired Cyp17a2-enhanced STING activity, as shown by reduced IFNφ1pro response and *vig1* transcripts (Fig. 6O and 6P). Additionally, *trim11* knockdown abolished Cyp17a2-mediated STING upregulation in endogenous and overexpression system (Fig. 6Q). These findings establish that Cyp17a2 recruits TRIM11 to catalyze K33-linked polyubiquitination, thereby stabilizing STING protein.

7. STING K203 is essential for Cyp17a2-mediated ubiquitination

The mechanism between TRIM11 and Cyp17a2 in STING stabilization was further characterized. TRIM11 overexpression was shown to intensify Cyp17a2-driven STING ubiquitination, while *trim11* knockdown attenuated this effect (Fig. 7A and 7B). Specific enhancement of K33-linked ubiquitination by TRIM11 was demonstrated, with reciprocal reduction upon TRIM11 abrogation (Fig. 7C and 7D). Mass spectrometry analysis identified K203 and K221 as candidate ubiquitination sites (Fig. 7E). Among generated lysine-to-arginine mutants (K203R, K221R), STING stabilization by Cyp17a2 was abolished specifically in K203R mutant (Fig. 7F). Corresponding loss of IFN induction and ubiquitination capacity were observed in K203R mutant (Fig. 7G-7I). K33-linked ubiquitination was specifically impaired in K203R but not K221R variants (Fig. 7J). TRIM11-mediated enhancement of WT and K33-specific ubiquitination was eliminated in K203R mutant (Fig. 7K and 7L). TRIM11 domain analysis was performed using RING/BBOX/SPRY deletion mutants (Fig. 7M). The SPRY domain was required for TRIM11-STING-Cyp17a2 interactions (Fig. 7N and 7O). Both RING and SPRY domains were essential for TRIM11-driven ubiquitination (Fig. 7P and 7Q). These data establish K203 as the critical ubiquitination site in STING and define RING/SPRY domains of TRIM11 as necessary for Cyp17a2-mediated stabilization.

8. Cyp17a2 Degrades SVCV P Protein Through Modulation of K33-Linked

Polyubiquitination

To determine whether Cyp17a2 directly engage in antiviral activity beyond regulating host immune responses, Co-IP assays were performed. Transient transfection experiments revealed specific interaction between Cyp17a2 and SVCV P protein, which was confirmed reciprocally (Fig. 8A and 8B). This interaction was further observed in SVCV-infected cells using P protein-specific antibody (Fig. 8C). In our antiviral trials, overexpression of Cyp17a2 led to a reduction in P protein levels during SVCV infection. Consequently, the investigation focused on whether Cyp17a2 could directly target the SVCV P protein for degradation. As anticipated, the co-expression of Cyp17a2 resulted in a decrease in the level of SVCV P protein Overexpression of Cyp17a2 reduced P protein levels during SVCV infection (Fig. 8D). Fluorescence microscopy confirmed diminished red fluorescent signals corresponding to SVCV P protein in Cyp17a2-expressing cells (Fig. 8E). Confocal microscopy analysis of SVCV P protein subcellular distribution revealed that the fluorescent signals from P-mCherry fusion constructs (red) showed partial co-localization with Cyp17a2 (green) in cytoplasmic compartments (Fig. 8F). To investigate degradation mechanisms, inhibitors targeting distinct pathways were tested. Cyp17a2-mediated P protein degradation was blocked by the proteasome inhibitor MG132, but not by autophagy inhibitors (3-MA, Baf-A1, CQ) (Fig. 8G). Ubiquitination assays demonstrated that Cyp17a2 significantly reduced P protein polyubiquitination (Fig. 8H). Mutation analysis using ubiquitin variants revealed that Cyp17a2 selectively decreased K33-linked polyubiquitination, as K33R mutants exhibited no significant changes, while K33-specific ubiquitination was markedly reduced (Fig. 8I and 8J). In contrast, knockdown of *cyp17a2* exhibited minimal impact on both WT-Ub and K33-linked polyubiquitination levels of the P protein (Fig. 8K). These findings demonstrate that Cyp17a2 promotes proteasomal degradation of the SVCV P protein by selectively attenuating K33-linked polyubiquitination, defining its role as an antiviral protein.

9. The K12 site of P protein is essential for Cyp17a2-mediated degradation

To investigate the specific molecular mechanism underlying ubiquitination-mediated degradation of the P protein, mass spectrometry analysis revealed ubiquitin-specific protease 7 (USP7) and USP8 as candidate deubiquitinating

enzymes (Fig. 9A). Both USP7 and USP8 were found to associate with the P protein, however, only USP8 interacted with Cyp17a2. Therefore, USP8 became the focus of subsequent study (Fig. 9B). The validity of these interactions was further confirmed through reciprocal experiments (Fig. 9C). Confocal microscopy analysis of USP8 subcellular localization demonstrated overlapping cytoplasmic co-localization between USP8-GFP (green fluorescence) and mCherry-tagged Cyp17a2 or the P protein (red fluorescence) (Fig. 9D). Cyp17a2 overexpression enhanced USP8 and P protein binding, whereas *cyp17a2* knockdown disrupted this interaction (Fig. 9E and 9F). USP8 overexpression amplified Cyp17a2-mediated P protein reduction (Fig. 9G). Knockdown of USP8 abolished Cyp17a2-dependent P protein degradation (Fig. 9H and 9I). USP8 facilitated Cyp17a2-induced deubiquitination of P protein, with knockdown reversing this effect (Fig. 9J). This result was also observed in the K33-linked ubiquitination assay (Fig. 9K). Mass spectrometry identified K12 as a critical lysine modification site (Fig. 9L). The K12R mutant resisted Cyp17a2-mediated degradation and showed impaired deubiquitination in WT ubiquitin and K33-linked assays (Fig. 9M and 9N). USP8 failed to enhance Cyp17a2-mediated deubiquitination in K12R mutants (Fig. 9O). Truncation analysis demonstrated that USP8 residues 1-301 aa or 734-1067 aa were essential for interactions with P protein and Cyp17a2 (Fig. 9P and 9Q). USP8 mutants only residues 1-301 aa or 302-733 aa lost the ability to support Cyp17a2-mediated P protein deubiquitination (Fig. 9R). These data establish that Cyp17a2 requires USP8 and the P protein K12 site to mediate deubiquitination-dependent degradation, with USP8 residues 734-1067 aa being indispensable for this process.

Discussion

The influence of biological sex on antiviral immunity presents striking evolutionary parallels and divergences across various species. While mammalian systems have been shown to establish the canonical paradigm of higher female immune competence through sex chromosome complement and hormonal regulation,

our findings in fish reveal an intriguing inversion of this trend. Contrary to the well-documented XX/XY-based sexual dimorphism in mammalian immunity, our study demonstrates that male zebrafish exhibit enhanced antiviral responses through an autosomal gene-mediated mechanism that challenges conventional understanding of sex-specific immunity and underscores the extraordinary evolutionary plasticity of teleost immune systems.

This sexual dichotomy in immune competence emerges against the backdrop of teleost's unparalleled diversity in sexual determination mechanisms. Unlike the chromosomal rigidity of mammalian systems, fish have evolved a spectrum of sex determination strategies ranging from conserved XX/XY systems in Japanese medaka (*Oryzias latipes*) and Nile tilapia (*Oreochromis niloticus*) to the tripartite X1Y1Y2 system of tiger characin (*Hoplias malabaricus*) and the ZZ/ZW system of half-smooth tongue sole (*Cynoglossus semilaevis*)[15]. Notably, this genomic plasticity extends beyond canonical sex chromosomes through the presence of naturally occurring polyploidy and accessory B chromosomes which observed in Lake Victoria cichlids (*Lithochromis rubripinnis*), as well as the 3–4 supernumerary microchromosomes of gibel carp, which mimic sex chromosome functionality through their tandem repeat-enriched, transposon-derived elements[16]. In addition, environmental factors can override genetically programmed sex determination in select fish species without chromosomal modifications, as exemplified by thermal stress-induced masculinization in XX Japanese medaka and Nile tilapia through androgen-driven developmental reprogramming[17]. This phenotypic plasticity coupled with extraordinary genomic diversity in sex determination systems, establishes teleost as unparalleled models for investigating the evolutionary continuum between genetic and environmental influences on sexual differentiation. It is evident that this complexity exceeds the capabilities of the mammalian mechanism, thereby necessitating meticulous mechanical analysis.

In this study, our mechanistic dissection reveals that enhanced male antiviral competence in zebrafish from elevated expression of the autosomal *cyp17a2* gene, operating through dual antiviral pathways. First, Cyp17a2 stabilizes the STING

protein via TRIM11-mediated K33-linked polyubiquitination at Lys203, amplifying IFN production. Second, it recruits USP8 to remove K33-linked ubiquitination at Lys12 of SVCV P protein, promoting its proteasomal degradation (Fig. 10). This dual functionality establishes Cyp17a2 as a central node in sex-specific antiviral regulation, functioning independently of canonical sex chromosome pathways. Particularly noteworthy is the demonstration that sexual dimorphism in immunity can arise through differential regulation of autosomal genes rather than direct sex chromosome effects - a mechanism distinct from mammalian X-linked immune gene dosage effects or estrogen-mediated immunomodulation. These discoveries in zebrafish, a species naturally lacking sex chromosomes, highlight one of the mechanisms underlying sex-specific antiviral immunity in teleost, demonstrating a system distinct from mammalian.

Sexual dimorphism in viral susceptibility represents a conserved yet mechanistically complex phenomenon across vertebrates. While males generally exhibit increased vulnerability to numerous viral pathogens such as dengue virus and influenza A virus, notable exceptions exist where females demonstrate higher susceptibility, including infections by herpes simplex virus and measles virus[2]. These divergent patterns underscore a dual dependency of sex-biased infection outcomes on both host immunological determinants and viral evolutionary strategies[1]. For instance, the male predominance observed in severe dengue virus cases may be explained by both gender-specific occupational exposure risks and sexual dimorphism in Ab-dependent enhancement mechanisms, potentially linked to androgen-mediated modulation of antiviral immune responses[18]. Whereas female susceptibility to herpes simplex virus could be related to ovarian sex hormones, including estradiol and progesterone[19]. Critically, sex differences in antiviral immunity are not static but evolve across the lifespan and are tightly linked to age and reproductive status[20]. For example, sex disparities in hantavirus infection outcomes emerge post-puberty, coinciding with hormonal maturation[21]. Similarly, during the 2009 H1N1 pandemic in Japan, morbidity rates exhibited a triphasic sex bias: males<20 and >80 years old showed higher susceptibility than females, whereas females of reproductive age (20-49 years) faced elevated risks[22]. This pattern aligns with the hypothesis that estrogen peaks during reproductive years enhance antiviral defenses in females, while

age-related declines in gonadal hormones may diminish this protective effect in postmenopausal populations[23]. Our study extends these principles to teleost species, revealing novel sex-specific resistance patterns in fish-virus interactions. Male zebrafish demonstrated heightened resistance to SVCV, while male crucian carp exhibited reduced susceptibility to CyHV-2[24]. These findings suggest that male-biased resistance may represent an evolutionarily conserved strategy in certain fish-virus system. However, whether this trend generalizes across all piscine viruses—or whether females conversely dominate resistance in specific viral contexts—remains unresolved.

STING was originally identified as a critical adaptor molecule mediating antiviral signaling cascades[25]. Subsequential studies have established its indispensable role in orchestrating innate immune responses against both DNA and RNA viral pathogens. Current mechanistic understanding reveals that upon detection of cytoplasmic pathogen-derived DNA, STING operates through two distinct molecular pathways: serving as a downstream effector of essential single-stranded/double-stranded DNA sensors or functioning as a direct receptor for microbial cyclic dinucleotides (CDNs). Following activation, this TM protein recruits and activates TBK1, which subsequently phosphorylates IRF3 to facilitate its nuclear translocation and initiate IFN production. Notably, the protein demonstrates functional pleiotropy in RNA viral infections through selective interaction with RIG-I rather than melanoma differentiation-associated protein 5 (MDA5), thereby activating parallel IRF3-dependent antiviral signaling pathways. Numerous studies indicate remarkable conservation of STING-mediated IFN induction mechanisms across teleost species[26]. Mechanism studies further reveal that fish STING maintains dual antiviral functionality against both nucleic acid virus types, while simultaneously being subjected to targeted manipulation by various viral pathogens as an immune evasion strategy.

The CYP450 enzyme superfamily exhibits multifaceted roles across species, encompassing physiological processes and immune regulation. In human immune cells, pharmacological inhibition of CYP1A has been demonstrated to upregulate the expression of stem cell factor receptor and interleukin 22, directly linking CYP1-dependent metabolism of environmental small molecules to immune modulation[27]. Evolutionary conservation of this regulatory mechanism is evident in teleost, where grass carp (*Ctenopharyngodon idella*) CYP1A demonstrates dynamic

expression during grass carp reovirus (GCRV) infection, implicating its role in antiviral immunity[28]. Our study further identifies Cyp17a2 as a sexually dimorphic regulator of IFN signaling in fish. This finding expands the recognized roles of the CYP450 superfamily in immune regulation, revealing a novel mechanism underlying sex-specific immunity in lower vertebrates.

In conclusion, zebrafish model with its lack of conserved sex chromosomes and environmental sex determination plasticity, provides unique insights into the evolutionary continuum of sexual dimorphism. Our results suggest that the relationship between sexual differentiation and immune competence may be more fluid in teleost than in mammals, potentially reflecting adaptive responses to aquatic pathogens and variable mating systems. Future investigations should explore whether this autosomal-centered mechanism represents a teleost specific adaptation or an ancestral feature subsequently modified in terrestrial vertebrates, while also examining potential interactions between environmental sex determinants and immune gene regulation.

Acknowledgment

We thank Fang Zhou (Institute of Hydrobiology, Chinese Academy of Sciences) for assistance with confocal microscopy analysis and Dr. Feng Xiong (China Zebrafish Resource Center, Institute of Hydrobiology, Chinese Academy of Sciences) for assistance with qPCR analysis.

This work was supported by the Strategic Priority Research Program of the Chinese Academy of Sciences (XDB0730300), Biological Breeding-National Science and Technology Major Project (2023ZD04065), National Excellent Youth Science Fund (32322086) and the Youth Innovation Promotion Association provided funding to Shun Li. National Key Research and Development Program of China (2023YFD2400201) provided funding to Dan-Dan Chen. National Natural Science Foundation of China (32173023) provided funding to Long-Feng Lu.

Declaration of interests

The authors declare no competing interests.

STAR Methods

Ethics statement

The experiments involved in this study were conducted in compliance with ethical regulations. The fish experiments were carried out under the guidance of the European Union Guidelines for the Handling of Laboratory Animals (2010/63/EU) and approved by the Ethics Committee for Animal Experiments of the Institute of Hydrobiology, Chinese Academy of Sciences (CAS) (No. 2024-069).

Fish, cells, and viruses

Mature zebrafish individuals 2.5 months after hatching (0.4 ± 0.1 g) were selected in this study. Wild-type (WT) zebrafish (AB strain; *Danio rerio*) were procured from the China Zebrafish Resource Center (CZRC), while *cyp17a2* mutant lines were generously provided by Dr. Zhan Yin's laboratory at the Institute of Hydrobiology, Chinese Academy of Sciences. All specimens were bred using standardized procedures. In accordance with the ethical requirements and national animal welfare guidelines, all experimental fish were required to undergo a two-week acclimatization period in the laboratory and have their health assessed prior to the commencement of the study. Only fish that appeared healthy and were mobile were selected for scientific investigation. ZF4 cells (American Type Culture Collection, ATCC) were cultured in Ham's F-12 medium (Invitrogen) supplemented with 10% fetal bovine serum (FBS) at 28˚C and 5% CO_2. EPC cells were obtained from the Chinese Culture Collection Centre for Type Cultures (CCTCC), Gibel carp brain (GiCB) cells were provided by Ling-Bing Zeng (Yangtze River Fisheries Research Institute, Chinese Academy of Fishery Sciences), these cells were maintained at 28°C in 5% CO_2 in medium 199 (Invitrogen) supplemented with 10% FBS. Spring viremia of carp virus (SVCV) was propagated in EPC cells until a cytopathogenic effect (CPE) was observed, and then cell culture fluid containing SVCV was harvested and centrifuged at 4×10^3 *g* for 20 min to remove the cell debris, and the supernatant was

stored at -80°C until used. Cyprinid herpesvirus 2 (CyHV-2, obtained from Yancheng city, Jiangsu province, China) was provided by Prof. Liqun Lu (Shanghai Ocean University). CyHV-2 was propagated in GICB cells and harvested in a similar way to SVCV.

Plasmid construction and reagents

The sequences of zebrafish and gibel carp (*Carassius gibelio*) Cyp17a2 (GenBank accession number: NM_001105670.1 and XM_026199804.1) were obtained from the National Centre for Biotechnology Information (NCBI) website. Cyp17a2 was amplified by polymerase chain reaction (PCR) using cDNA from adult zebrafish or gibel carp tissues as a template and cloned into the expression vector pCMV-HA or pCMV-Myc (Clontech) vectors. Zebrafish MAVS (NM_001080584.2), TBK1 (NM_001044748.2), STING (NM_001278837.1) and the truncated mutants of STING, IRF3 (NM_001143904.1), IRF7 (BC058298.1), TRIM11 (XM_021470074.1) and the truncated mutants of TRIM11, TRAIP (NM_205607.1), SOCS3a (NM_199950.1), USP7 (XM_021473871.1), USP8 (XM_009293353.4), and N, P, and G protein (DQ097384.2) of SVCV were cloned into pCMV-Myc and pCMV-Tag2C vectors. The shRNA of *Pimephales promelas* Cyp17a2 (XM_039679078.1), STING (HE856620.1), and USP8 (XM_039680290.1) were designed by BLOCK-iT RNAi Designer and cloned into the pLKO.1-TRC Cloning vector. For subcellular localization experiments, Cyp17a2 was constructed onto pEGFP-N3 (Clontech), while STING and P protein were constructed onto pCS2-mCherry (Clontech). The plasmids containing zebrafish IFNφ1pro-Luc and ISRE-Luc in the pGL3-Basic luciferase reporter vector (Promega) were constructed as described previously. The *Renilla* luciferase internal control vector (pRL-TK) was purchased from Promega. The ubiquitin mutant expression plasmids Lys-33/63 (all lysine residues were mutated except Lys-33 or Lys-63) and Lys-33R/63R (only Lys-33 or Lys-63 mutated) were ligated into the pCMV-HA vectors named Ub-K33O/K63O-HA and Ub-K33R/K63R. All constructs were confirmed by DNA sequencing. Polyinosinic-polycytidylic acid (poly I:C) was purchased from Sigma-Aldrich used at a final concentration of 1 μg/μl. MG132 (Cat. No. M7449), 3-Methyladenine (3-MA) (Cat. No. M9281), Chloroquine

(CQ) (Cat. No. C6628) were obtained from Sigma-Aldrich. Bafilomycin A1 (Baf-A1) (Cat. No. S1413) and Cycloheximide (CHX) (NSC-185) were obtained from Selleck.

Transcriptomic analysis

Total RNA was extracted using the TRIzol method and evaluated for RNA purity and quantification using a NanoDrop 2000 spectrophotometer (Thermo Scientific, Waltham, U.S.A.) and RNA integrity was assessed using an Agilent 2100 Bioanalyzer (Agilent Technologies, Santa Clara, U.S.A.). Transcriptome sequencing and data analysis were conducted by OE Biotech (Shanghai, China). The raw sequencing data was submitted to the NCBI (GEO accession number: GSE286486).

Transient transfection and virus infection

EPC cells were transfected in 6-well and 24-well plates using transfection reagents from FishTrans (MeiSenTe Biotechnology) according to the manufacturer's protocol. Antiviral assays were conducted in 24-well plates by transfecting EPC cells with the plasmids shown in the figure. At 24 h post-transfection, cells were infected with SVCV at a multiplicity of infection (MOI = 0.001). After 24 h, supernatant aliquots were harvested for detection of virus titers, the cell monolayers were fixed by 4% paraformaldehyde (PFA) and stained with 1% crystal violet for visualizing CPE. For virus titration, 200 μl of culture medium were collected at 48 h post-infection and used for detection of virus titers according to the method of Reed and Muench. The supernatants were subjected to 3-fold or 10-fold serial dilutions and then added (100 μl) onto a monolayer of EPC cells cultured in a 96-well plate. After 48 or 72 h, the medium was removed and the cells were washed with phosphate-buffered saline (PBS), fixed by 4% PFA, and stained with 1% crystal violet. The virus titer was expressed as 50% tissue culture infective dose ($TCID_{50}$/ml). For viral infection, fish were anesthetized with methanesulfonate (MS-222) and intraperitoneally (i.p.) injected with 5 μl of M199 containing SVCV (5×10^8 $TCID_{50}$/ml). The i.p. injection of PBS was used as mock infection. Then the fish were migrated into the aquarium containing new aquatic water.

Luciferase activity assay

EPC cells were cultured overnight in 24-well plates and subsequently

co-transfected with the expression plasmid and luciferase reporter plasmid. The cells were infected with SVCV or transfected with poly I:C for 24 h prior to harvest. At 24 h post-stimulation, cells were washed with PBS and lysed for measuring luciferase activity by the Dual-Luciferase Reporter Assay System (Promega) according to the manufacturer's instructions. Firefly luciferase activity was normalized based on the *Renilla* luciferase activity.

RNA extraction, reverse transcription, and quantitative PCR (qPCR)

The RNA was extracted using TRIzol reagent (Invitrogen), and first-strand cDNA was synthesized with a PrimeScript RT kit with gDNA Eraser (Takara). qPCR was performed on the CFX96 Real-Time System (Bio-Rad) using SYBR green PCR Master Mix (Yeasen). The PCR conditions were as follows: 95°C for 5 min and then 40 cycles of 95°C for 20 s, 60°C for 20 s, and 72°C for 20 s. The primers utilized for the qPCRs are presented in Table S1, and the *β-actin* gene was utilized as the internal control. The relative fold changes were calculated by comparison to the corresponding controls using the $2^{-\Delta\Delta Ct}$ method (where CT was the threshold cycle).

Co-immunoprecipitation (Co-IP) assay

EPC cells were cultured in 10-cm^2 dishes overnight and subsequently transfected with 10 μg plasmid as illustrated. At 24 h post-transfection, the medium was removed and cells were washed with PBS. Then the cells were lysed in 1 ml radioimmunoprecipitation (RIPA) lysis buffer [1% NP-40, 50 mM Tris-HCl, pH 7.5, 150 mM NaCl, 1 mM EDTA, 1 mM NaF, 1 mM sodium orthovanadate (Na_3VO_4), 1 mM phenyl-methylsulfonyl fluoride (PMSF), 0.25% sodium deoxycholate] containing protease inhibitor cocktail (Sigma-Aldrich) at 4°C for 1 h on a rocker platform. The cellular debris was removed by centrifugation at 12,000 × *g* for 15 min at 4°C. The supernatant was transferred to a fresh tube and incubated with 20 μl anti-Flag/HA/Myc affinity gel (Sigma-Aldrich) overnight at 4°C with constant rotating incubation. These samples were further analyzed by immunoblotting (IB). Immunoprecipitated proteins were collected by centrifugation at 5000 × *g* for 1 min at 4°C, washed three times with lysis buffer and resuspended in 50 μl 2 × SDS sample buffer. The immunoprecipitates and whole cell lysates (WCLs) were analyzed by IB

with the indicated antibodies (Abs).

***In vivo* ubiquitination assay**

The transfected EPC cells were washed twice with 10 mL ice-cold PBS and subsequently digested with 1 mL 0.25% trypsin-EDTA (1×) (Invitrogen) for 2-3 min until the cells were dislodged. 100 μL FBS was added to neutralize the trypsin and the cells were resuspended into 1.5 mL centrifuge tube, centrifuged at 2000 × *g* for 5 min. The supernatant was discarded and the cell precipitations were resuspended using 1 mL PBS and centrifuged at 2000 × *g* for 5 min. The collected cell precipitations were lysed using 100 μL PBS containing 1% SDS and denatured by heating for 10 min. The supernatants were diluted with lysis buffer until the concentration of SDS was reduced to 0.1%. The diluted supernatants were incubated with 20 μL anti-Myc affinity gel overnight at 4°C with constant agitation. Subsequently, these samples were subjected to further analysis by IB. The immunoprecipitated proteins were collected by centrifugation at 5000 × *g* for 1 min at 4°C, washed for three times with lysis buffer and resuspended in 100 μL 1× SDS sample buffer.

Immunoblot analysis

Immunoprecipitates or WCLs were analyzed as described previously. Abs were diluted as follows: anti-*β-actin* (ABclonal, AC026) at 1:10000, anti-Flag (Sigma-Aldrich, F1804) at 1:3000, anti-HA (Covance, MMS-101R) at 1:3000, anti-Myc (Santa Cruz Biotechnology, sc-40) at 1:3000, anti-TRIM11 (ABclonal, A13887) at 1:1000, anti-USP8 (proteintech, 27791-1-AP) at 1:1000, and HRP-conjugated anti-mouse/rabbit IgG (Thermo Scientific, 31430/31460) at 1:5000, anti-N/P/G/STING/ (prepared and purified in our lab) at 1:2000.

Immunofluorescence (IF)

EPC cells were plated onto glass coverslips in 6-well plates and infected with SVCV (MOI = 1) 24 h. The cells were then washed with PBS and fixed in 4% PFA at room temperature for 1 h and permeabilized with 0.2% Triton X-100 in ice-cold PBS for 15 min. The samples were incubated for 1 h at room temperature in PBS containing 2% bovine serum albumin (BSA, Sigma-Aldrich). After additional PBS washing, the samples were incubated with anti-N Ab in PBS containing 2% BSA for

2-4 h at room temperature. After three times washed by PBS, the samples were incubated with secondary Ab (Goat anti-Rabbit IgG (H+L) Highly Cross-Adsorbed Secondary Antibody, Alexa Fluor™ Plus 488) (Thermo Scientific, A32731, 1:5000) in PBS containing 2% BSA for 1 h at room temperature. After additional PBS washing, the cells were finally stained with 1 μg/ml 4′, 6-diamidino-2-phenylindole (DAPI, Beyotime Institute of Biotechnology, Shanghai, China) for 10 min in the dark at room temperature. Finally, the coverslips were washed and observed with a confocal microscope under a 10× immersion objective (SP8; Leica).

Fluorescent microscopy

EPC cells were plated onto coverslips in 6-well plates and transfected with the plasmids indicated for 24 h. Thereafter, the cells were washed twice with PBS and fixed with 4% PFA for 1 h. After being washed three times with PBS, the cells were stained with 1 μg/ml DAPI for 15 min in the dark at room temperature. Subsequently, the coverslips were washed and observed with a confocal microscope under a 63× oil immersion objective (SP8; Leica).

Histopathology

Liver and spleen tissues from three individuals of control or virus-infected fish at 2 days post infection (dpi) were dissected, and fixed in Bouin's Fixative overnight. Subsequently, the samples were dehydrated in ascending grades of alcohol and embedded into paraffin. Sections at 5 μm thickness were taken and stained with hematoxylin and eosin (H&E). Histological changes were examined by optical microscopy at ×40 magnification and were analyzed by the Aperio ImageScope software.

Statistics analysis

For fish survival analysis, Kaplan-Meier survival curves were generated and subsequently subjected to a log-rank test. For the bar graph, one representative experiment of at least three independent experiments is shown, and each was done in triplicate. For the dot plot graph, each dot point represents one independent biological replicate. Unpaired Student's t test was used for statistical analysis. Data are presented as mean ± standard error of the mean (SEM). A p value < 0.05 was considered

statistically significant.

References

[1] S. L. Klein, S. Huber, in (Eds.: S. L. Klein, C. Roberts), Springer Berlin Heidelberg, Berlin, Heidelberg **2010**.

[2] S. L. Klein, *BioEssays : news and reviews in molecular, cellular and developmental biology* **2012**, *34* (12), 1050, https://doi.org/10.1002/bies.201200099.

[3] G. Health, Icrw, Aphrc, A. Gautam, *The-COVID-19-Sex-Disaggregated-Data-Tracker-Update*, **2020**.

[4] a) D. Guha-Sapir, B. Schimmer, *Emerg Themes Epidemiol* **2005**, *2* (1), 1, https://doi.org/10.1186/1742-7622-2-1; b) P. K. Tsay, D. I. Tai, Y. M. Chen, C. P. Yu, S. Y. Wan, Y. J. Shen, D. Y. Lin, *Chang Gung medical journal* **2009**, *32* (2), 155; c) A. I. Burguete-García, C. J. Conde-González, R. Jiménez-Méndez, Y. Juárez-Díaz, E. Meda-Monzón, K. Torres-Poveda, V. Madrid-Marina, *Salud publica de Mexico* **2011**, *53 Suppl 1*, S7.

[5] S. M. Liva, R. R. Voskuhl, *Journal of immunology* **2001**, *167* (4), 2060, https://doi.org/DOI 10.4049/jimmunol.167.4.2060.

[6] a) I. Pinheiro, L. Dejager, C. Libert, *BioEssays : news and reviews in molecular, cellular and developmental biology* **2011**, *33* (11), 791, https://doi.org/10.1002/bies.201100047; b) S. Sharma, M. Eghbali, *Biology of sex differences* **2014**, *5* (1), 3, https://doi.org/10.1186/2042-6410-5-3.

[7] S. Akira, S. Uematsu, O. Takeuchi, *Cell* **2006**, *124* (4), 783, https://doi.org/10.1016/j.cell.2006.02.015.

[8] S. N. Chen, P. F. Zou, P. Nie, *Immunology* **2017**, *151* (1), 16, https://doi.org/10.1111/imm.12714.

[9] a) H. Ishikawa, G. N. Barber, *Nature* **2008**, *455* (7213), 674, https://doi.org/10.1038/nature07317; b) G. X. Ni, Z. Ma, B. Damania, *PLoS pathogens* **2018**, *14* (8), https://doi.org/ARTN e1007148 10.1371/journal.ppat.1007148.

[10] a) S. Aguirre, A. M. Maestre, S. Pagni, J. R. Patel, T. Savage, D. Gutman, K. Maringer, D. Bernal-Rubio, R. S. Shabman, V. Simon, J. R. Rodriguez-Madoz, L. C. F. Mulder, G. N. Barber, A. Fernandez-Sesma, *PLoS pathogens* **2012**, *8* (10), https://doi.org/ARTN e100293410.1371/journal.ppat.1002934; b) A. Nazmi, R. Mukhopadhyay, K. Dutta, A. Basu, *Scientific reports* **2012**, *2*, https://doi.org/ARTN 34710.1038/srep00347; c) F. P. You, P. H. Wang, L. Yang, G. Yang, Y. O. Zhao, F. Qian, W. Walker, R. Sutton, R. Montgomery, R. T. Lin, A. Iwasaki, E. Fikrig, *Nature immunology* **2013**, *14* (12), 1237, https://doi.org/10.1038/ni.2756.

[11] L. Lau, E. E. Gray, R. L. Brunette, D. B. Stetson, *Science* **2015**, *350* (6260), 568, https://doi.org/10.1126/science.aab3291.

[12] Y. M. Kim, M. Kang, J. H. Choi, B. H. Lee, G. H. Kim, J. H. Ohn, S. Y. Kim, M. S. Park, H. W. Yoo, *Metabolism* **2014**, *63* (1), 42, https://doi.org/10.1016/j.metabol.2013.08.015.

[13] L. Y. Zhou, D. S. Wang, T. Kobayashi, A. Yano, B. Paul-Prasanth, A. Suzuki, F. Sakai, Y. Nagahama, *Endocrinology* **2007**, *148* (9), 4282, https://doi.org/10.1210/en.2007-0487.

[14] S. C. Shi, T. T. Shu, X. Li, Q. Y. Lou, X. Jin, J. Y. He, Z. Yin, G. Zhai, *Front Endocrinol* **2022**, *13*, https://doi.org/ARTN 91063910.3389/fendo.2022.910639.

[15] a) M. Matsuda, Y. Nagahama, A. Shinomiya, T. Sato, C. Matsuda, T. Kobayashi, C. E. Morrey, N. Shibata, S. Asakawa, N. Shimizu, H. Hori, S. Hamaguchi, M. Sakaizumi, *Nature* **2002**, *417* (6888), 559, https://doi.org/DOI 10.1038/nature751; b) M. H. Li, Y. L. Sun, J. E. Zhao, H. J. Shi, S. Zeng, K. Ye, D. N. Jiang, L. Y. Zhou, L. N. Sun, W. J. Tao, Y. Nagahama, T. D. Kocher, D. S. Wang, *Plos Genet* **2015**, *11* (11), https://doi.org/ARTN e100567810.1371/journal.pgen.1005678; c) M. B. Cioffi, L. A. C. Bertollo, *Heredity* **2010**, *105* (6), 554, https://doi.org/10.1038/hdy.2010.18; d) S. L. Chen, G. J. Zhang, C. W. Shao, Q. F. Huang, G. Liu, P. Zhang, W. T. Song, N. An, D. Chalopin, J. N. Volff, Y. H. Hong, Q. Y. Li, Z. X. Sha, H. L. Zhou, M. S. Xie, Q. L. Yu, Y. Liu, H. Xiang, N. Wang, K. Wu, C. G. Yang, Q. Zhou, X. L. Liao, L. F. Yang, Q. M. Hu, J. L. Zhang, L. Meng, L. J. Jin, Y. S. Tian, J. M. Lian, J. F. Yang, G. D. Miao, S. S. Liu, Z. Liang, F. Yan, Y. Z. Li, B. Sun, H. Zhang, J. Zhang, Y. Zhu, M. Du, Y. W. Zhao, M. Schartl, Q. S. Tang, J. Wang, *Nature Genetics* **2014**, *46* (3), 253, https://doi.org/10.1038/ng.2890.

[16] a) K. Yoshida, Y. Terai, S. Mizoiri, M. Aibara, H. Nishihara, M. Watanabe, A. Kuroiwa, H. Hirai, Y. Hirai, Y. Matsuda, N. Okada, *Plos Genet* **2011**, *7* (8), https://doi.org/ARTN e100220310.1371/journal.pgen.1002203; b) X. Y. Li, Q. Y. Zhang, J. Zhang, L. Zhou, Z. Li, X. J. Zhang, D. Wang, J. F. Gui, *Genetics* **2016**, *203* (3), 1415, https://doi.org/10.1534/genetics.115.185843.

[17] a) Y. Hayashi, H. Kobira, T. Yamaguchi, E. Shiraishi, T. Yazawa, T. Hirai, Y. Kamei, T. Kitano, *Mol Reprod Dev* **2010**, *77* (8), 679, https://doi.org/10.1002/mrd.21203; b) S. Poonlaphdecha, E. Pepey, M. Canonne, H. de Verdal, J. F. Baroiller, H. D'Cotta, *Gen Comp Endocr* **2013**, *193*, 234, https://doi.org/10.1016/j.ygcen.2013.06.007.

[18] E. S. Gan, D. H. R. Ting, K. R. Chan, *Expert Rev Anti-Infe* **2017**, *15* (2), 111, https://doi.org/10.1080/14787210.2017.1254550.

[19] A. Wald, *Herpes : the journal of the IHMF* **2004**, *11 Suppl 3*, 130A.

[20] S. L. Klein, K. L. Flanagan, *Nature Reviews Immunology* **2016**, *16* (10), 626, https://doi.org/10.1038/nri.2016.90.

[21] P. A. Vial, M. Ferres, C. Vial, J. Klingström, C. Ahlm, R. López, N. Le Corre, G. Mertz, *Lancet Infect Dis* **2023**, *23* (9), E371, https://doi.org/10.1016/S1473-3099(23)00128-7.

[22] N. Eshima, O. Tokumaru, S. Hara, K. Bacal, S. Korematsu, M. Tabata, S. Karukaya, Y. Yasui, N. Okabe, T. Matsuishi, *PloS one* **2011**, *6* (4), https://doi.org/ARTNe1940910.1371/journal.pone.0019409.

[23] J. Cui, Y. Shen, R. Li, *Trends Mol Med* **2013**, *19* (3), 197, https://doi.org/10.1016/j.molmed.2012.12.007.

[24] L. F. Lu, J. Y. Jiang, W. X. Du, X. L. Wang, Z. C. Li, X. Y. Zhou, C. Zhang, C. Y. Mou, D. D. Chen, Z. Li, L. Zhou, J. F. Gui, X. Y. Li, S. Li, *PLoS pathogens* **2022**, *18* (6), https://doi.org/ARTNe101062610.1371/journal.ppat.1010626.

[25] Y. Ran, H. B. Shu, Y. Y. Wang, *Cytokine Growth F R* **2014**, *25* (6), 631, https://doi.org/10.1016/j.cytogfr.2014.05.003.

[26] a) Y. Huang, Z. Ouyang, W. Wang, Y. Yu, P. Li, S. Zhou, S. Wei, J. Wei, X. Huang, Q. Qin, *Fish Shellfish Immunol* **2015**, *47* (1), 157, https://doi.org/10.1016/j.fsi.2015.09.014; b) S. Biacchesi, E. Merour, A. Lamoureux, J. Bernard, M. Bremont, *PloS one* **2012**, *7* (10), e47737, https://doi.org/10.1371/journal.pone.0047737; c) F. Sun, Y. B. Zhang, T. K. Liu, J. Shi, B. Wang, J. F. Gui, *J. Immunol.* **2011**, *187* (5), 2531, https://doi.org/10.4049/jimmunol.1100642.

[27] R. Effner, J. Hiller, S. Eyerich, C. Traidl-Hoffmann, K. Brockow, M. Triggiani, H. Behrendt, C. B. Schmidt-Weber, J. T. M. Buters, *Scientific reports* **2017**, *7*, https://doi.org/ARTN4400510.1038/srep44005.

[28] P. F. Chu, L. B. He, D. H. Zhu, R. Huang, L. J. Liao, Y. M. Li, Z. Y. Zhu, Y. P. Wang, *Fish Shellfish Immun* **2019**, *95*, 35, https://doi.org/10.1016/j.fsi.2019.10.022.

Figure legends

Figure 1. Male fish show stronger viral resistance than females

(A) Survival (Kaplan-Meier Curve) of male and female zebrafish (n = 15 per group) at various days after i.p. injected with SVCV (5×10^8 $TCID_{50}$/ml, 5 μL/individual). (B) Sex-specific morphological alterations in zebrafish given i.p. injection of SVCV for 48 h (n = 3 per group). (C) Microscopy of H&E-stained liver and spleen sections from male and female zebrafish treated with SVCV for 48 h. (D) IF analysis of SVCV-N protein in liver and spleen of male and female zebrafish treated with SVCV for 48 h. (E) qPCR analysis of *svcv-n* mRNA in the liver and spleen of male and female zebrafish (n = 26 per group) given i.p. injection of SVCV for 48 h. (F) IB analysis of SVCV proteins in the liver and spleen sections of male and female zebrafish (n = 7

per group) treated with SVCV for 48 h. (G) The viral titer of heart in male and female zebrafish (n = 40 per group) treated with SVCV for 48 h.

Figure 2. Male-biased cyp17a2 regulates RLR-mediated antiviral immunity

(A) Schematic representation of zebrafish tissue dissection and RNA extraction for transcriptome sequencing. The head-kidney from male and female zebrafish. Total RNAs were extracted and used for transcriptome sequencing and analysis. (B) The differently expressed gene number of mRNA variations in head-kidney of male and female zebrafish. (C) Heatmap view of mRNA variations of sex-regulated genes in the head-kidney of male and female zebrafish. (D) qPCR analysis of *cyp17a2* mRNA in the head-kidney of male and female zebrafish (n = 50 per group). (E) qPCR analysis of *cyp17a2* mRNA in the brain, heart, head-kidney, gill, liver, spleen, body-kidney, gonad, gut, muscle, and skin of male and female zebrafish (n = 5 per group). (F) IB analysis of Cyp17a2 in the heart, head-kidney, gill, liver, spleen, body-kidney, gonad, and skin of male and female zebrafish (n = 5 per group). (G) qPCR analysis of *cyp17a2* mRNA in the ZF4 or EPC cells infected with SVCV for the indicated times. (H) IB analysis of Cyp17a2 in ZF4 and EPC cells infected with SVCV for the indicated times. (I) Survival (Kaplan-Meier Curve) of *cyp17a2*$^{+/+}$ and *cyp17a2*$^{-/-}$ male zebrafish (n = 16 per group) at various days after i.p. injected with SVCV (5×10^8 TCID50/ml, 5 μl/individual). (J) Microscopy of H&E-stained liver and spleen sections from *cyp17a2*$^{+/+}$ and *cyp17a2*$^{-/-}$ male zebrafish treated with SVCV for 48 h. (K) IF analysis of SVCV-N protein in the liver and spleen of *cyp17a2*$^{+/+}$ and *cyp17a2*$^{-/-}$ male zebrafish treated with SVCV for 48 h. (L) The viral titer of heart in *cyp17a2*$^{+/+}$ and *cyp17a2*$^{-/-}$ male zebrafish (n = 15 per group) treated with SVCV for 48 h. (M) qPCR analysis of *svcv-n* mRNA in the liver and spleen of *cyp17a2*$^{+/+}$ and *cyp17a2*$^{-/-}$ male zebrafish (n = 20 per group) given i.p. injection of SVCV for 48 h. (N) IB analysis of SVCV proteins in the liver and spleen sections of *cyp17a2*$^{+/+}$ and *cyp17a2*$^{-/-}$ male zebrafish (n = 3 per group) treated with SVCV for 48 h. (O) KEGG pathway enrichment map showing the top 10 signaling pathways of total. (P) GSEA of differentially expressed genes in the liver of *cyp17a2*$^{+/+}$ and *cyp17a2*$^{-/-}$male

zebrafish infected with SVCV and enrichment of RLR signaling pathway. The *p*-values were corrected for the False Discovery Rate (FDR) method, and modules with *p*-values less than 0.05 were selected as significant. (Q) qPCR analysis of *ifnφ1* mRNA in the liver and spleen of *cyp17a2*$^{+/+}$ and *cyp17a2*$^{-/-}$ male zebrafish (n = 20 per group) given i.p. injection of SVCV for 48 h.

Figure 3. Cyp17a2 upregulates IFN expression and inhibits viral replication

(A-C and G) Luciferase activity of IFNφ1pro, IFNφ3pro, and ISRE in EPC cells transfected with indicated plasmids for 24 h, and then untreated or transfected with poly I:C (0.5 μg) or infected with SVCV (MOI = 1) for 24 h before luciferase assays. (D) qPCR analysis of *cyp17a2* in EPC cells transfected with indicated plasmids for 24 h, and then untreated or transfected with poly I:C (2 μg) or infected with SVCV (MOI = 1) for 24 h. (E and F) IB analysis of proteins in EPC cells transfected with indicated plasmids for 24 h. (H) Heatmap view of mRNA variations of SVCV-activated ISG sets in the Cyp17a2-overexpressing cells or *cyp17a2* knockdown cells and infected with SVCV. (I) qPCR analysis of *ifn* and *vig1* in EPC cells transfected with indicated plasmids for 24 h, and then untreated or infected with SVCV (MOI = 1) for 24 h. (J and K) Plaque assay of virus titers in EPC cells or GICB cells transfected with indicated plasmids for 24 h, followed by SVCV or CyHV-2 challenge for 24 h or 48 h. (L and M) qPCR and IB analysis of SVCV genes in EPC cells transfected with indicated plasmids for 24 h, followed by SVCV challenge for 24 h. (N and O) IF analysis of SVCV proteins in EPC cells transfected with indicated plasmids for 24 h, followed by SVCV challenge for 24 h.

Figure 4. Cyp17a2 physically interacts with STING and stabilizes its expression

(A-C and E) IB analysis of WCLs and proteins immunoprecipitated with anti- Flag or HA Ab-conjugated agarose beads from EPC cells transfected with indicated plasmids for 24 h. (D) Schematic representation of full-length STING and its mutants. (F and G) Confocal microscopy of Cyp17a2 and ER or STING and its mutants in EPC cells

transfected with indicated plasmids for 24 h. The coefficient of colocalization was determined by qualitative analysis of the fluorescence intensity of the selected area in Merge. (H) qPCR analysis of *sting* in EPC cells transfected with indicated plasmids for 24 h, followed by untreated or infected with SVCV (MOI = 1) for 24 h. (I) IB analysis of proteins in EPC cells transfected with indicated plasmids for 24 h. (J) Fluorescent analysis of proteins in EPC cells transfected with indicated plasmids for 24 h. The fluorescence intensity (arbitrary unit, a.u.) was recorded by the LAS X software, and the data were expressed as mean ± SD, n = 5. (K) IB analysis of proteins in EPC cells transfected with indicated plasmids for 24 h, followed by untreated or infected with transfected with poly I:C (2 μg) or SVCV (MOI = 1) for 24 h. (L-N) IB analysis of proteins in EPC cells transfected with indicated plasmids for 18 h, then treated with CHX for 4 h and 8 h.

Figure 5. Cyp17a2 potentiates STING-induced IFN production and antiviral responses

(A-D) Luciferase activity of IFNφ1pro and ISRE in EPC cells transfected with indicated plasmids for 24 h before luciferase assays. (E and F) qPCR analysis of *ifn* and *vig1* in EPC cells transfected with indicated plasmids for 24 h. (G, H, and M) Plaque assay of virus titers in EPC cells transfected with indicated plasmids for 24 h and then infected with SVCV (MOI = 1) for 24 h. (I and N) qPCR analysis of SVCV genes in EPC cells transfected with indicated plasmids for 24 h, followed by SVCV challenge for 24 h. (J and Q) IB analysis of proteins in EPC cells transfected with indicated plasmids for 24 h and then untreated or infected with SVCV (MOI = 1) for 24 h. (K, O, and P) IF analysis of N protein and P protein in EPC cells transfected with indicated plasmids for 24 h, followed by SVCV challenge for 24 h. The fluorescence intensity (arbitrary unit, a.u.) was recorded by the LAS X software, and the data were expressed as mean ± SD, n = 5. (L) IB analysis of proteins in EPC cells transfected with indicated plasmids for 24 h.

Figure 6. Cyp17a2 stabilizes STING by orchestrating TRIM11-catalyzed K33-linked polyubiquitination

(A) IB analysis of proteins in EPC cells transfected with indicated plasmids for 18 h, then treated with CHX and DMSO, MG132, or CQ for 4 h and 8 h. (B-D) STING ubiquitination assays in EPC cells transfected with indicated plasmids for 24 h. (E-G, J) IB analysis of WCLs and proteins immunoprecipitated with anti-Flag Ab-conjugated agarose beads from EPC cells transfected with indicated plasmids for 24 h. (H and I) Confocal microscopy of TRIM11 and ER or STING or Cyp17a2 in EPC cells transfected with indicated plasmids for 24 h. The coefficient of colocalization was determined by qualitative analysis of the fluorescence intensity of the selected area in Merge. (K and L, O and P) Luciferase activity of IFNφ1pro and qPCR analysis of *vig1* in EPC cells transfected with indicated plasmids for 24 h. (M and N, Q) IB analysis of proteins in EPC cells transfected with indicated plasmids for 24 h.

Figure 7 Cyp17a2-mediated ubiquitination of STING is dependent on the K203

(A-D, I-L, and P-Q) STING ubiquitination assays in EPC cells transfected with indicated plasmids for 24 h. (E) Mass spectrometry analysis of a peptide derived from ubiquitinated STING-Myc. (F) IB analysis of proteins in EPC cells transfected with indicated plasmids for 24 h. (G and H) Luciferase activity of IFNφ1pro and qPCR analysis of *ifn1* in EPC cells transfected with indicated plasmids for 24 h. (M) Schematic representation of full-length TRIM11 and its mutants. (N and O) IB of WCLs and proteins immunoprecipitated with anti-Flag/HA Ab-conjugated agarose beads from EPC cells transfected with indicated plasmids for 24 h.

Figure 8 Cyp17a2 induces proteasomal degradation of the SVCV P protein by catalyzing K33-linked polyubiquitination

(A-C) IB analysis of WCLs and proteins immunoprecipitated with anti-Flag, anti-HA, or anti-Myc Ab-conjugated agarose beads from EPC cells transfected with indicated

plasmids for 24 h. (D) IB analysis of proteins in EPC cells transfected with indicated plasmids for 24 h. (E) Fluorescent analysis of proteins in EPC cells transfected with indicated plasmids for 24 h. (F) Confocal microscopy of P and Cyp17a2 in EPC cells transfected with indicated plasmids for 24 h. The coefficient of colocalization was determined by qualitative analysis of the fluorescence intensity of the selected area in Merge. (G) IB analysis of proteins in EPC cells transfected with indicated plasmids for 18 h, followed by treatments of MG132 (10 μM), 3-MA (2 mM), Baf-A1 (100 nM), and CQ (50 μM) for 6 h, respectively. (H-K) P protein ubiquitination assays in EPC cells transfected with indicated plasmids for 18 h, followed by MG132 treatments for 6 h.

Figure 9 Cyp17a2 targets the K12 site of the P protein for K33-linked polyubiquitination

(A) List of proteins interacting with P protein detected by mass spectrometry. (B and C, E and F) IB analysis of WCLs and proteins immunoprecipitated with anti-HA, anti-Flag, or anti-Myc Ab-conjugated agarose beads from EPC cells transfected with indicated plasmids for 24 h. (D) Confocal microscopy of USP8 and Cyp17a2 or P protein in EPC cells transfected with indicated plasmids for 24 h. The coefficient of colocalization was determined by qualitative analysis of the fluorescence intensity of the selected area in Merge. (G-I and M) IB analysis of proteins in EPC cells transfected with indicated plasmids for 24 h. (J and K, N and O, R) P protein ubiquitination assays in EPC cells transfected with indicated plasmids for 18 h, followed by MG132 treatments for 6 h. (L) Mass spectrometry analysis of a peptide derived from ubiquitinated P-Myc. (P) Schematic representation of full-length USP8 and its mutants.

Figure 10 A mechanistic model illustrating the dual regulatory roles of Cyp17a2 in upregulating STING expression and degrading SVCV P protein

Upon virus infection, male-biased autosomal gene *cyp17a2* enhances antiviral

responses in males. Mechanistically, Cyp17a2, an ER-localized protein, stabilizes STING expression through recruitment of the E3 ubiquitin ligase TRIM11, promoting K33-linked polyubiquitination. Furthermore, Cyp17a2 facilitates proteasomal degradation of the SVCV P protein by engaging USP8 to reduce its K33-linked polyubiquitination, thereby amplifying antiviral IFN responses.

Figure S1 The differently expressed gene number of mRNA variations in liver of *cyp17a2*$^{+/+}$ and *cyp17a2*$^{-/-}$ male zebrafish infected with SVCV.

Figure S2 Heatmap view of mRNA variations of RLR-mediated ISGs sets in the liver of *cyp17a2*$^{+/+}$ and *cyp17a2*$^{-/-}$ male zebrafish infected with SVCV.

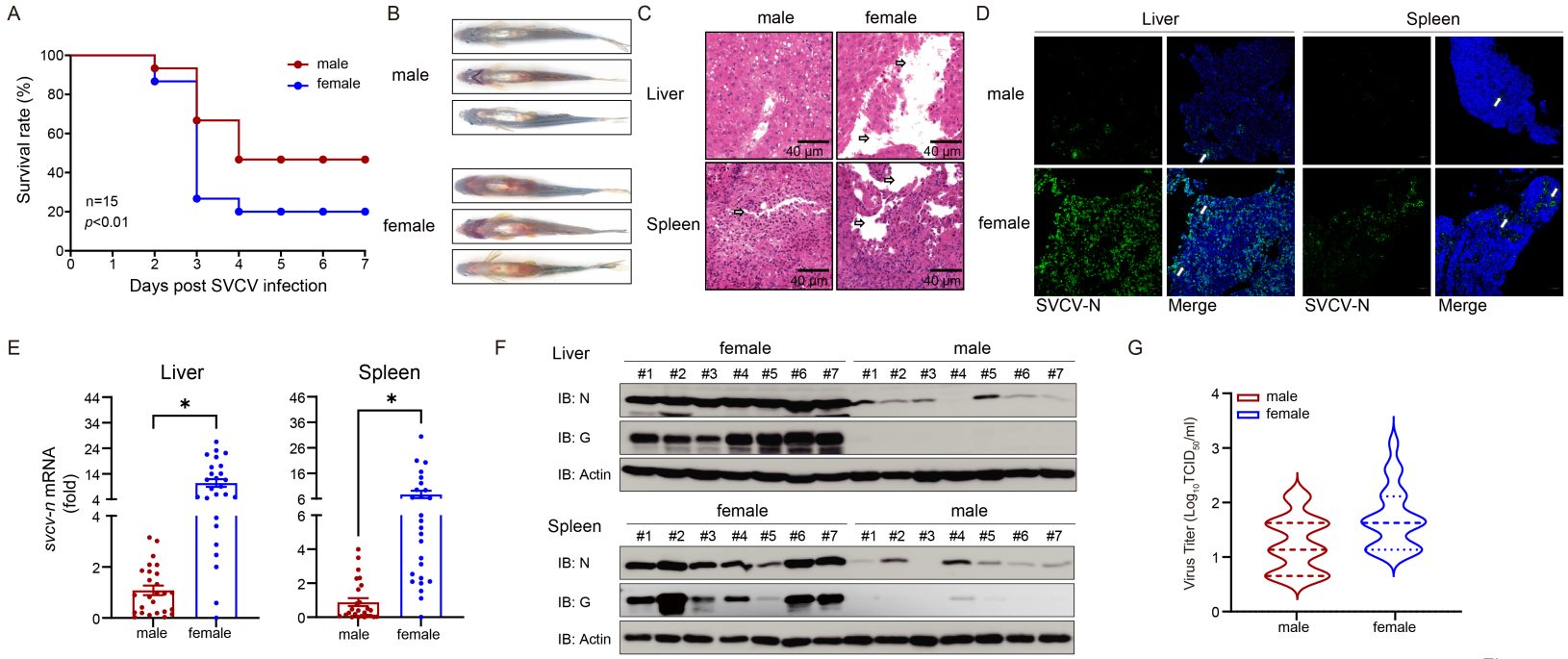
A
Survival rate (%)
Days post SVCV infection
male
female
n=15
p<0.01
B
male
female
C
male
female
Liver
Spleen
40 μm
D
Liver
Spleen
male
female
SVCV-N
Merge
E
Liver
Spleen
svcv-n mRNA (fold)
male
female
F
Liver
Spleen
female
male
IB: N
IB: G
IB: Actin
G
Virus Titer (Log10TCID50/ml)
male
female

Figure 1

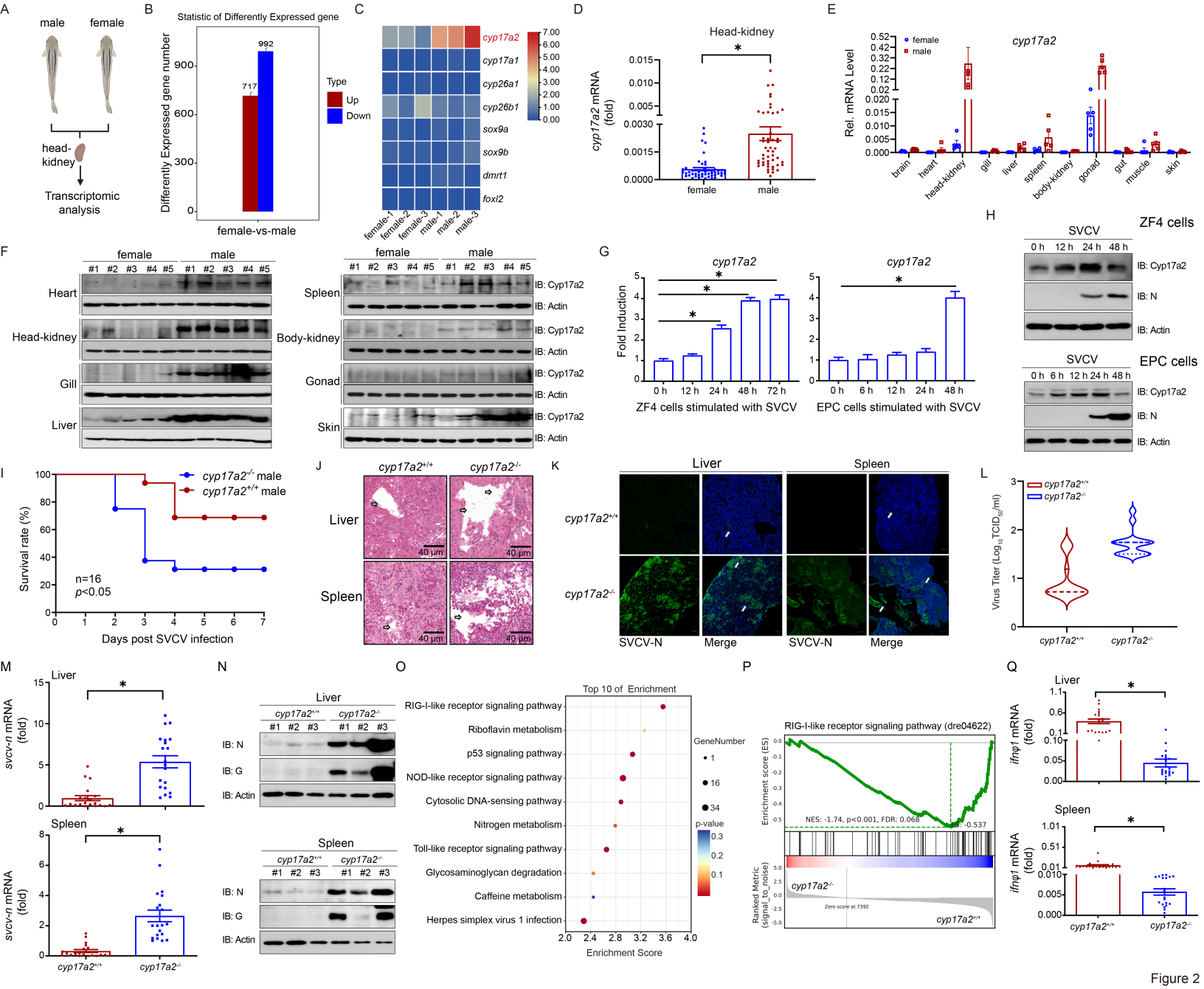
A
male
female
head-kidney
Transcriptomic analysis
B
Statistic of Differently Expressed gene
Differently Expressed gene number
992
717
Type
Up
Down
female-vs-male
C
cyp17a2
cyp17a1
cyp26a1
cyp26b1
sox9a
sox9b
dmrt1
foxl2
female-1
female-2
female-3
male-1
male-2
male-3
D
Head-kidney
cyp17a2 mRNA (fold)
female
male
E
cyp17a2
Rel. mRNA Level
female
male
brain
heart
head-kidney
gill
liver
spleen
body-kidney
gonad
gut
muscle
skin
F
female
male
Heart
Head-kidney
Gill
Liver
Spleen
Body-kidney
Gonad
Skin
IB: Cyp17a2
IB: Actin
G
cyp17a2
Fold Induction
ZF4 cells stimulated with SVCV
EPC cells stimulated with SVCV
H
ZF4 cells
SVCV
IB: Cyp17a2
IB: N
IB: Actin
EPC cells
I
cyp17a2-/- male
cyp17a2+/+ male
Survival rate (%)
n=16
p<0.05
Days post SVCV infection
J
cyp17a2+/+
cyp17a2-/-
Liver
Spleen
40 μm
K
Liver
Spleen
SVCV-N
Merge
L
Virus Titer (Log10TCID50/ml)
M
Liver
Spleen
svcv-n mRNA (fold)
N
Liver
Spleen
IB: N
IB: G
IB: Actin
O
Top 10 of Enrichment
RIG-I-like receptor signaling pathway
Riboflavin metabolism
p53 signaling pathway
NOD-like receptor signaling pathway
Cytosolic DNA-sensing pathway
Nitrogen metabolism
Toll-like receptor signaling pathway
Glycosaminoglycan degradation
Caffeine metabolism
Herpes simplex virus 1 infection
GeneNumber
p-value
Enrichment Score
P
RIG-I-like receptor signaling pathway (dre04622)
Enrichment score (ES)
NES: -1.74, p<0.001, FDR: 0.068
Ranked Metric (signal_to_noise)
Zero score at 7392
Q
Liver
Spleen
ifnφ1 mRNA (fold)

Figure 2

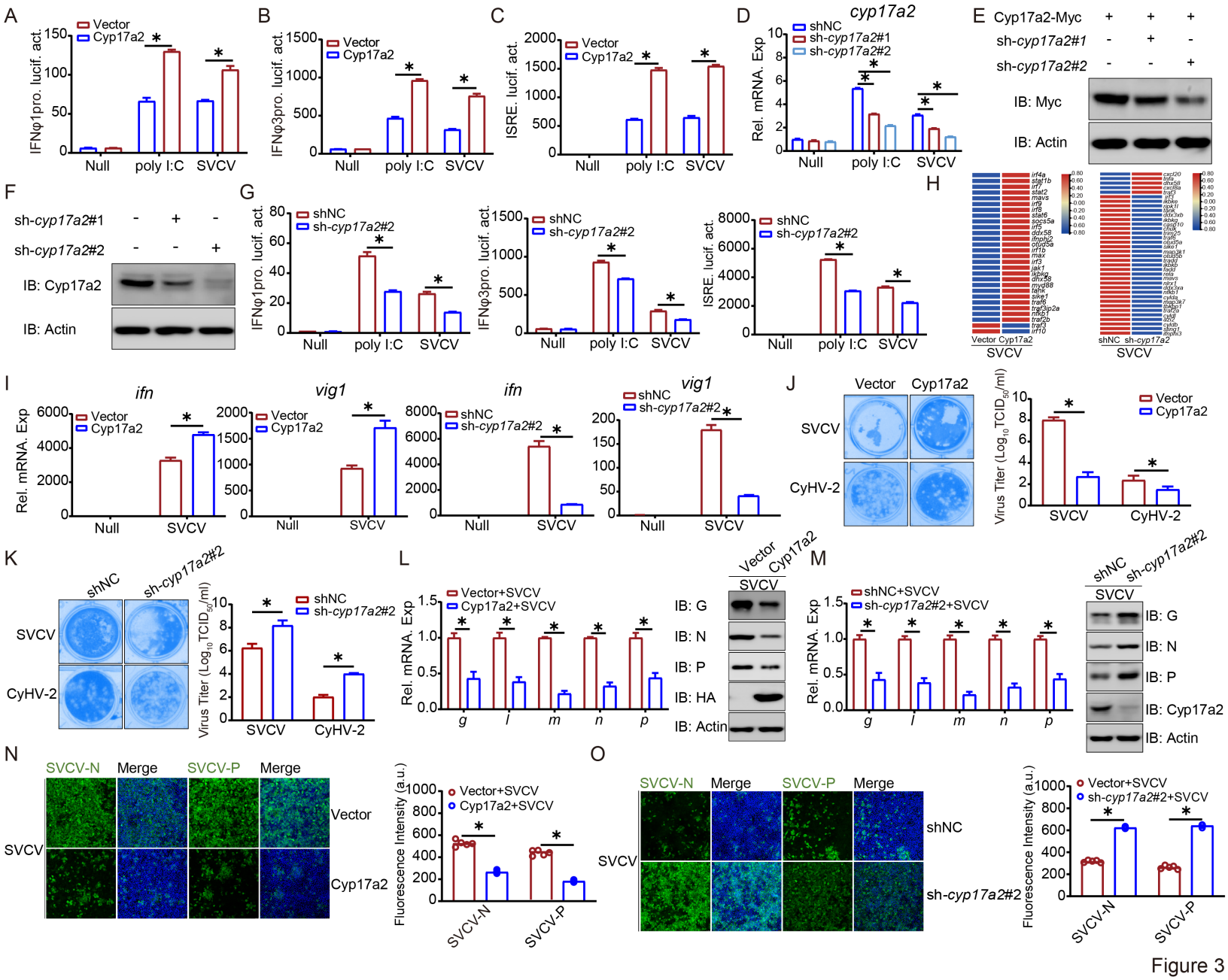
A
Vector
Cyp17a2
IFNφ1pro. lucif. act.
Null
poly I:C
SVCV
B
IFNφ3pro. lucif. act.
C
ISRE. lucif. act.
D
cyp17a2
shNC
sh-cyp17a2#1
sh-cyp17a2#2
Rel. mRNA. Exp
E
Cyp17a2-Myc
IB: Myc
IB: Actin
F
IB: Cyp17a2
G
H
I
ifn
vig1
J
CyHV-2
Virus Titer (Log10 TCID50/ml)
K
L
Rel. mRNA. Exp
IB: G
IB: N
IB: P
IB: HA
IB: Actin
M
N
SVCV-N
Merge
SVCV-P
Fluorescence Intensity (a.u.)
O

Figure 3

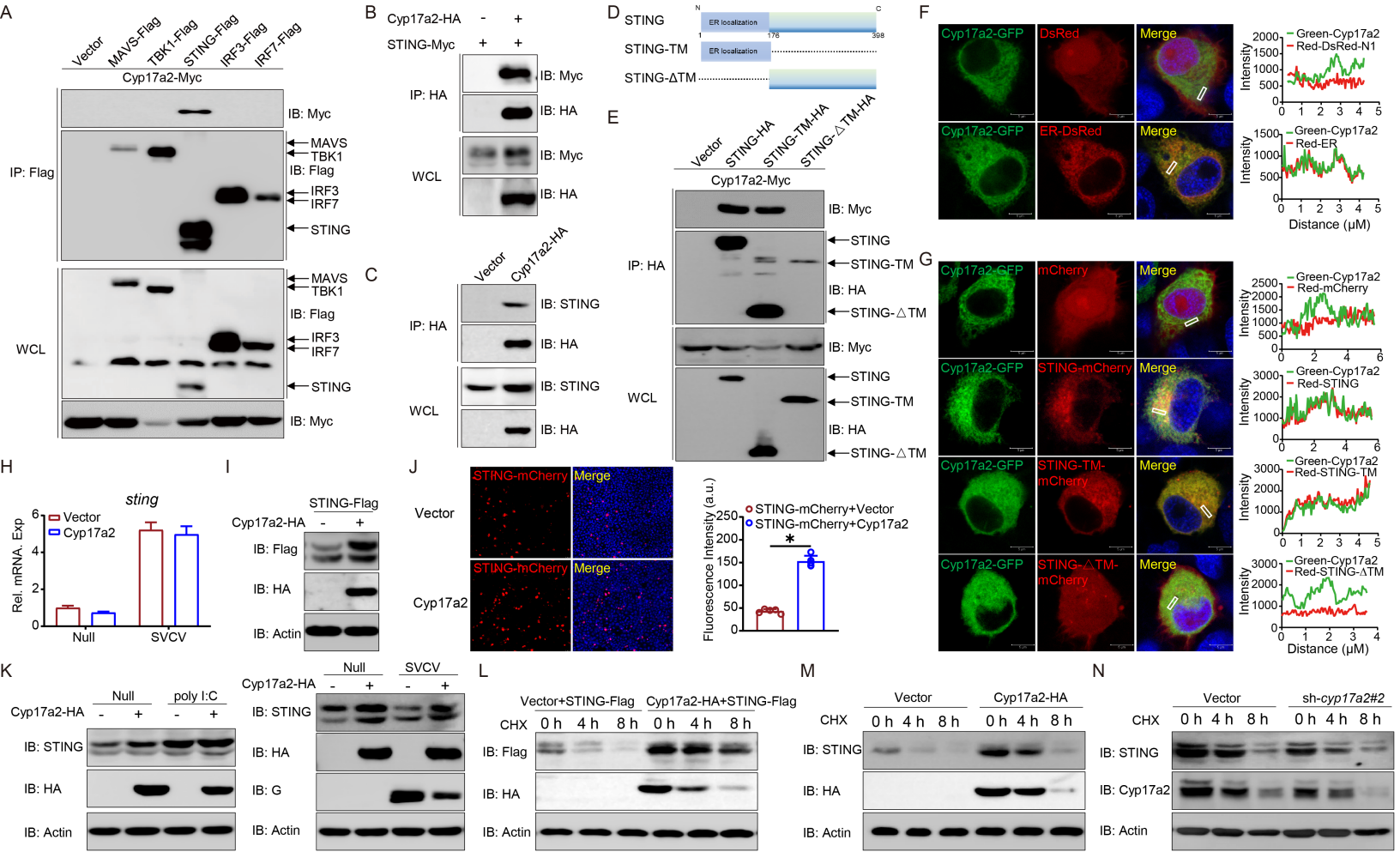
A
Vector
MAVS-Flag
TBK1-Flag
STING-Flag
IRF3-Flag
IRF7-Flag
Cyp17a2-Myc
IP: Flag
WCL
IB: Myc
MAVS
TBK1
IB: Flag
IRF3
IRF7
STING
B
Cyp17a2-HA
STING-Myc
IP: HA
WCL
IB: Myc
IB: HA
C
Vector
Cyp17a2-HA
IB: STING
D
STING
STING-TM
STING-ΔTM
ER localization
N
C
1
176
398
E
Vector
STING-HA
STING-TM-HA
STING-△TM-HA
Cyp17a2-Myc
STING-TM
STING-△TM
F
Cyp17a2-GFP
DsRed
ER-DsRed
Merge
Green-Cyp17a2
Red-DsRed-N1
Red-ER
Intensity
Distance (μM)
G
mCherry
STING-mCherry
STING-TM-mCherry
STING-△TM-mCherry
Red-mCherry
Red-STING
Red-STING-TM
Red-STING-ΔTM
H
sting
Vector
Cyp17a2
Rel. mRNA. Exp
Null
SVCV
I
STING-Flag
Cyp17a2-HA
IB: Flag
IB: HA
IB: Actin
J
STING-mCherry
Merge
Vector
Cyp17a2
STING-mCherry+Vector
STING-mCherry+Cyp17a2
Fluorescence Intensity (a.u.)
K
Null
poly I:C
Cyp17a2-HA
IB: STING
IB: HA
IB: Actin
IB: G
L
Vector+STING-Flag
Cyp17a2-HA+STING-Flag
CHX
0 h
4 h
8 h
IB: Flag
M
Vector
Cyp17a2-HA
N
sh-cyp17a2#2
IB: Cyp17a2

Figure 4

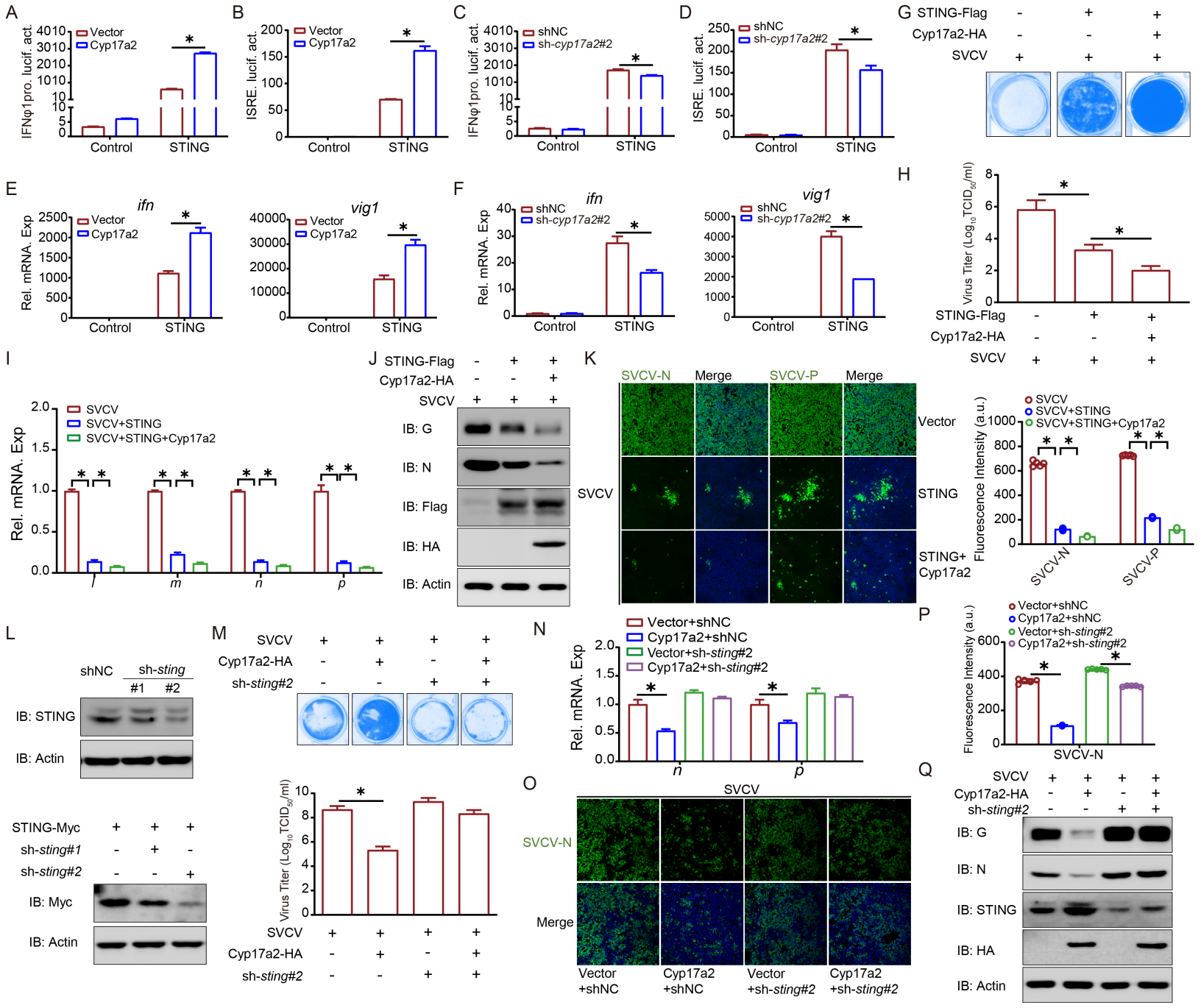
A
IFNφ1pro. lucif. act.
Vector
Cyp17a2
Control
STING
B
ISRE. lucif. act.
C
shNC
sh-cyp17a2#2
D
G
STING-Flag
Cyp17a2-HA
SVCV
E
ifn
vig1
Rel. mRNA. Exp
F
H
Virus Titer (Log10TCID50/ml)
I
SVCV
SVCV+STING
SVCV+STING+Cyp17a2
l
m
n
p
J
IB: G
IB: N
IB: Flag
IB: HA
IB: Actin
K
SVCV-N
Merge
SVCV-P
Vector
STING
STING+ Cyp17a2
Fluorescence Intensity (a.u.)
L
shNC
sh-sting
#1
#2
IB: STING
IB: Actin
STING-Myc
sh-sting#1
sh-sting#2
IB: Myc
M
N
Vector+shNC
Cyp17a2+shNC
Vector+sh-sting#2
Cyp17a2+sh-sting#2
O
Vector +shNC
Cyp17a2 +shNC
Vector +sh-sting#2
Cyp17a2 +sh-sting#2
P
Q

Figure 5

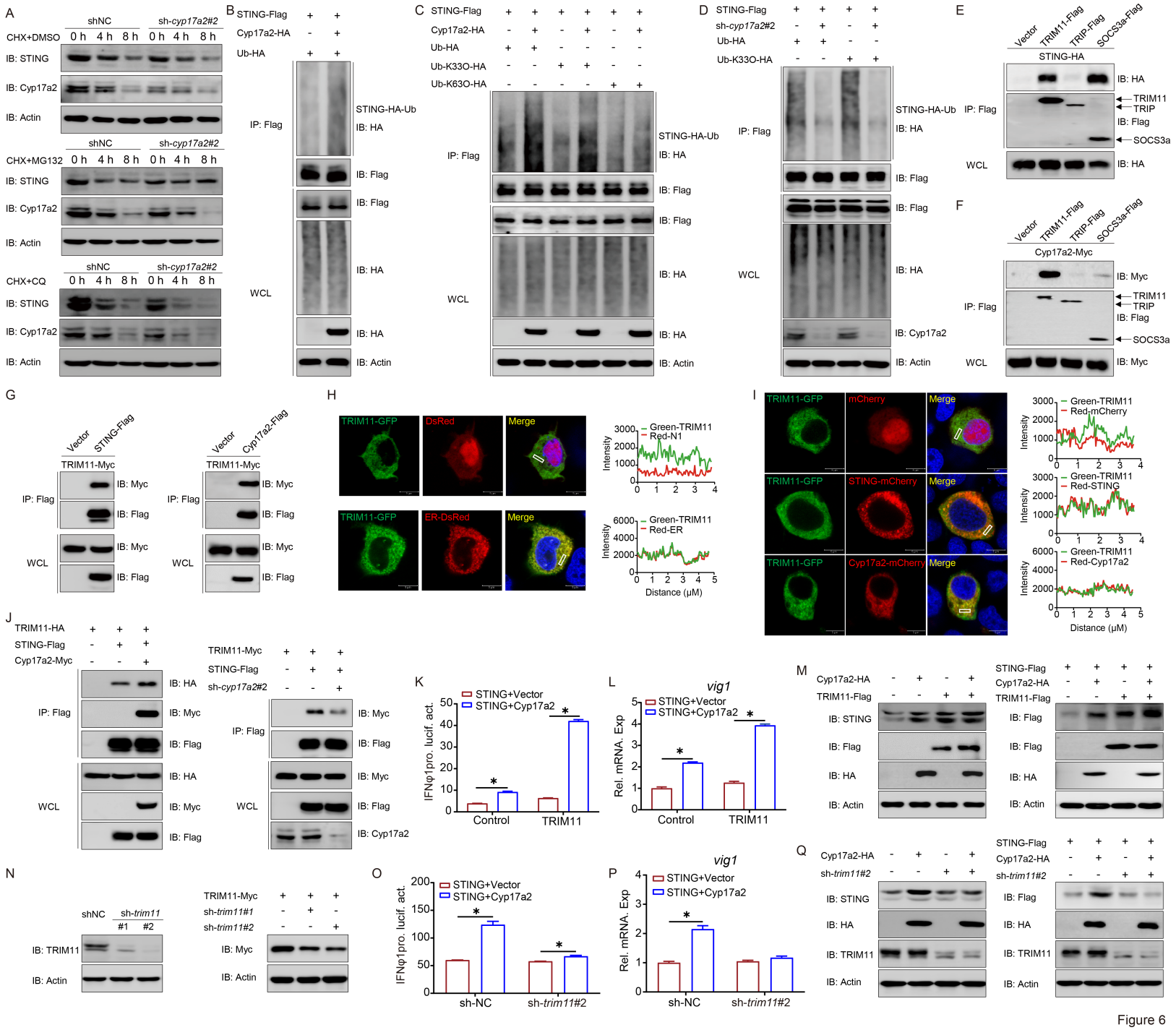
A
shNC
sh-cyp17a2#2
CHX+DMSO
0 h 4 h 8 h 0 h 4 h 8 h
IB: STING
IB: Cyp17a2
IB: Actin
CHX+MG132
CHX+CQ
B
STING-Flag
Cyp17a2-HA
Ub-HA
IP: Flag
STING-HA-Ub
IB: HA
IB: Flag
WCL
IB: Actin
C
Ub-K33O-HA
Ub-K63O-HA
D
sh-cyp17a2#2
E
Vector
TRIM11-Flag
TRIP-Flag
SOCS3a-Flag
STING-HA
TRIM11
TRIP
SOCS3a
F
Cyp17a2-Myc
IB: Myc
G
TRIM11-Myc
H
TRIM11-GFP
DsRed
Merge
ER-DsRed
Green-TRIM11
Red-N1
Red-ER
Intensity
Distance (μM)
I
mCherry
STING-mCherry
Cyp17a2-mCherry
Red-mCherry
Red-STING
Red-Cyp17a2
J
TRIM11-HA
Cyp17a2-Myc
IB: Cyp17a2
K
STING+Vector
STING+Cyp17a2
IFNφ1pro. lucif. act.
Control
TRIM11
L
vig1
Rel. mRNA. Exp
M
Cyp17a2-HA
TRIM11-Flag
IB: STING
IB: Flag
IB: HA
IB: Actin
N
shNC
sh-trim11
#1
#2
IB: TRIM11
sh-trim11#1
sh-trim11#2
O
sh-NC
P
Q

Figure 6

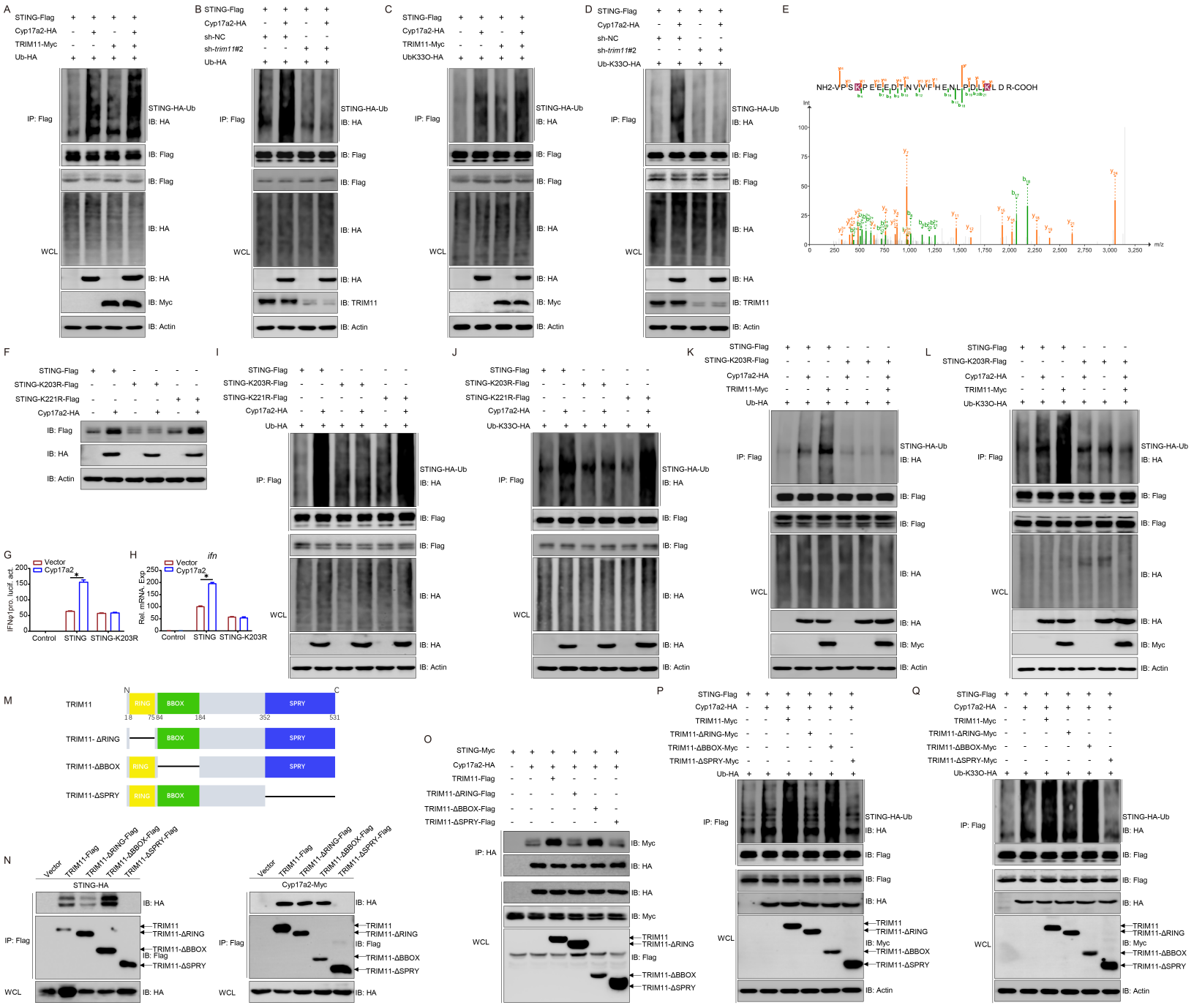
A
STING-Flag
Cyp17a2-HA
TRIM11-Myc
Ub-HA
IP: Flag
STING-HA-Ub
IB: HA
IB: Flag
WCL
IB: Myc
IB: Actin
B
sh-NC
sh-trim11#2
IB: TRIM11
C
UbK33O-HA
D
Ub-K33O-HA
E
NH2-VPSKPEEEDTNVVFHENLPDLKLDR-COOH
Int
m/z
F
STING-K203R-Flag
STING-K221R-Flag
G
Vector
Cyp17a2
IFNφ1pro. lucif. act.
Control
STING
STING-K203R
H
ifn
Rel. mRNA Exp.
I
J
K
L
M
TRIM11
N
C
RING
BBOX
SPRY
TRIM11- ΔRING
TRIM11-ΔBBOX
TRIM11-ΔSPRY
N
Vector
TRIM11-Flag
TRIM11-ΔRING-Flag
TRIM11-ΔBBOX-Flag
TRIM11-ΔSPRY-Flag
STING-HA
Cyp17a2-Myc
O
STING-Myc
TRIM11-Flag
TRIM11-ΔRING-Flag
TRIM11-ΔBBOX-Flag
TRIM11-ΔSPRY-Flag
P
TRIM11-ΔRING-Myc
TRIM11-ΔBBOX-Myc
TRIM11-ΔSPRY-Myc
Q

Figure 7

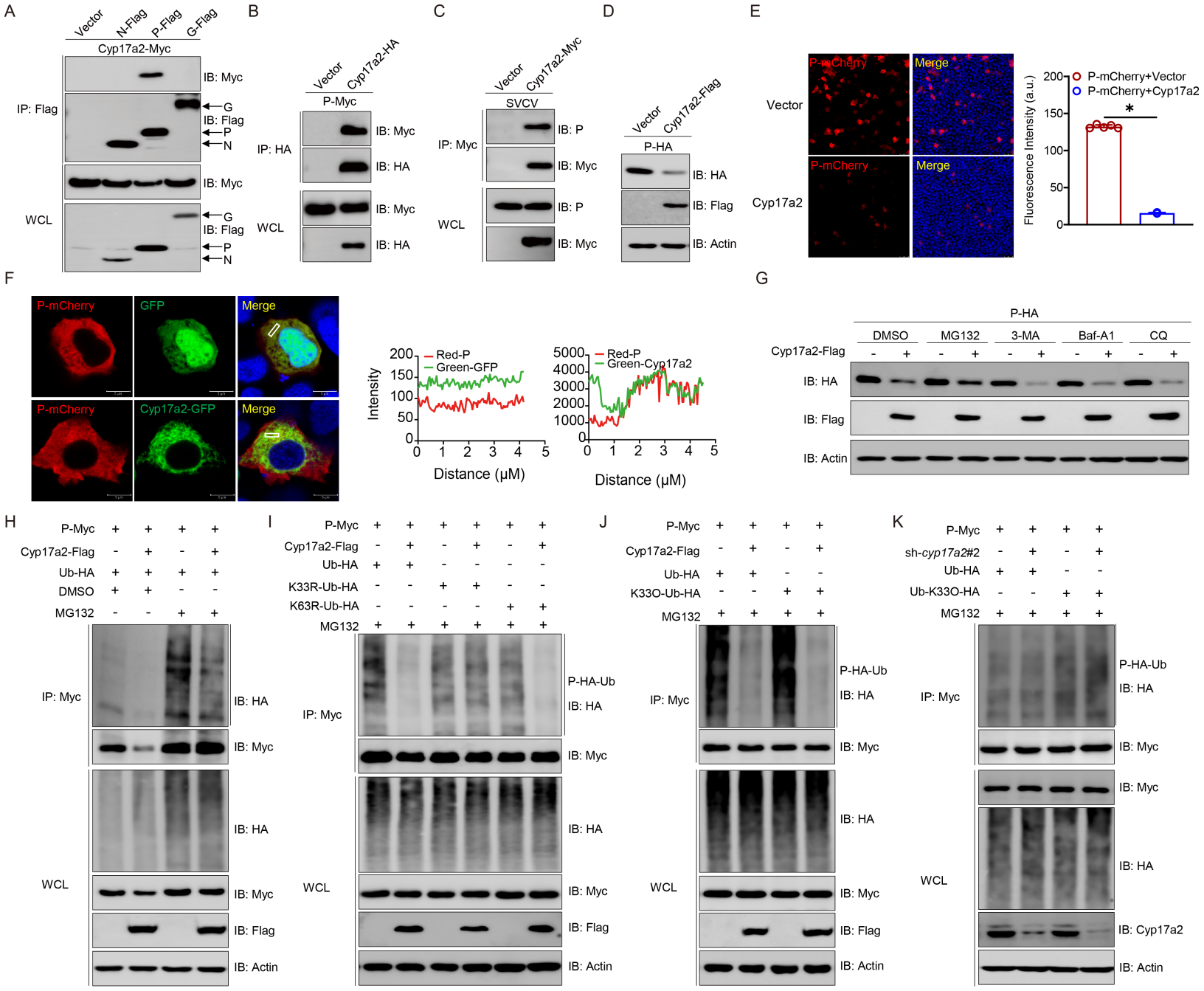
A
Vector
N-Flag
P-Flag
G-Flag
Cyp17a2-Myc
IP: Flag
IB: Myc
G
IB: Flag
P
N
IB: Myc
WCL
G
IB: Flag
P
N
B
Vector
Cyp17a2-HA
P-Myc
IP: HA
IB: Myc
IB: HA
WCL
IB: Myc
IB: HA
C
Vector
Cyp17a2-Myc
SVCV
IP: Myc
IB: P
IB: Myc
WCL
IB: P
IB: Myc
D
Vector
Cyp17a2-Flag
P-HA
IB: HA
IB: Flag
IB: Actin
E
Vector
Cyp17a2
P-mCherry
Merge
P-mCherry
Merge
Fluorescence Intensity (a.u.)
P-mCherry+Vector
P-mCherry+Cyp17a2
*
F
P-mCherry
GFP
Merge
P-mCherry
Cyp17a2-GFP
Merge
Intensity
Red-P
Green-GFP
Distance (μM)
Red-P
Green-Cyp17a2
Distance (μM)
G
P-HA
DMSO
MG132
3-MA
Baf-A1
CQ
Cyp17a2-Flag
IB: HA
IB: Flag
IB: Actin
H
P-Myc
Cyp17a2-Flag
Ub-HA
DMSO
MG132
IP: Myc
IB: HA
IB: Myc
WCL
IB: HA
IB: Myc
IB: Flag
IB: Actin
I
P-Myc
Cyp17a2-Flag
Ub-HA
K33R-Ub-HA
K63R-Ub-HA
MG132
IP: Myc
P-HA-Ub
IB: HA
IB: Myc
WCL
IB: HA
IB: Myc
IB: Flag
IB: Actin
J
P-Myc
Cyp17a2-Flag
Ub-HA
K33O-Ub-HA
MG132
IP: Myc
P-HA-Ub
IB: HA
IB: Myc
WCL
IB: HA
IB: Myc
IB: Flag
IB: Actin
K
P-Myc
sh-cyp17a2#2
Ub-HA
Ub-K33O-HA
MG132
IP: Myc
P-HA-Ub
IB: HA
IB: Myc
WCL
IB: Myc
IB: HA
IB: Cyp17a2
IB: Actin

Figure 8

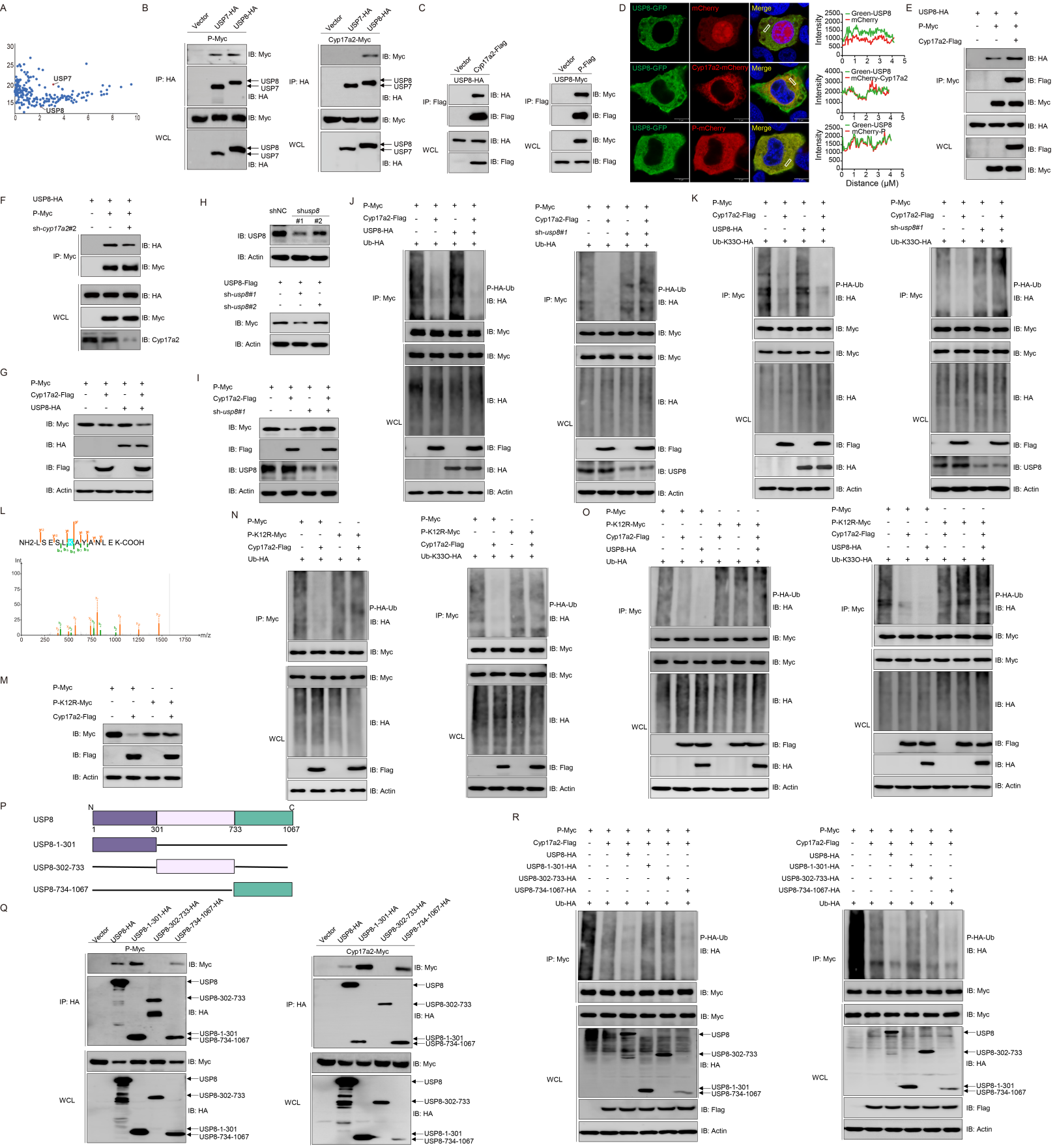
A
USP7
USP8
B
Vector
USP7-HA
USP8-HA
P-Myc
Cyp17a2-Myc
IP: HA
WCL
IB: Myc
IB: HA
USP8
USP7
C
Vector
Cyp17a2-Flag
P-Flag
USP8-HA
USP8-Myc
IP: Flag
IB: Flag
D
USP8-GFP
mCherry
Merge
Cyp17a2-mCherry
P-mCherry
Green-USP8
mCherry
mCherry-Cyp17a2
mCherry-P
Intensity
Distance (μM)
E
USP8-HA
P-Myc
Cyp17a2-Flag
IP: Myc
F
sh-cyp17a2#2
IB: Cyp17a2
H
shNC
shusp8
#1
#2
IB: USP8
IB: Actin
USP8-Flag
sh-usp8#1
sh-usp8#2
G
I
J
Ub-HA
P-HA-Ub
K
Ub-K33O-HA
L
NH2-L S E S L K A Y A N L E K-COOH
m/z
M
P-K12R-Myc
N
O
P
USP8
USP8-1-301
USP8-302-733
USP8-734-1067
Q
R

Figure 9

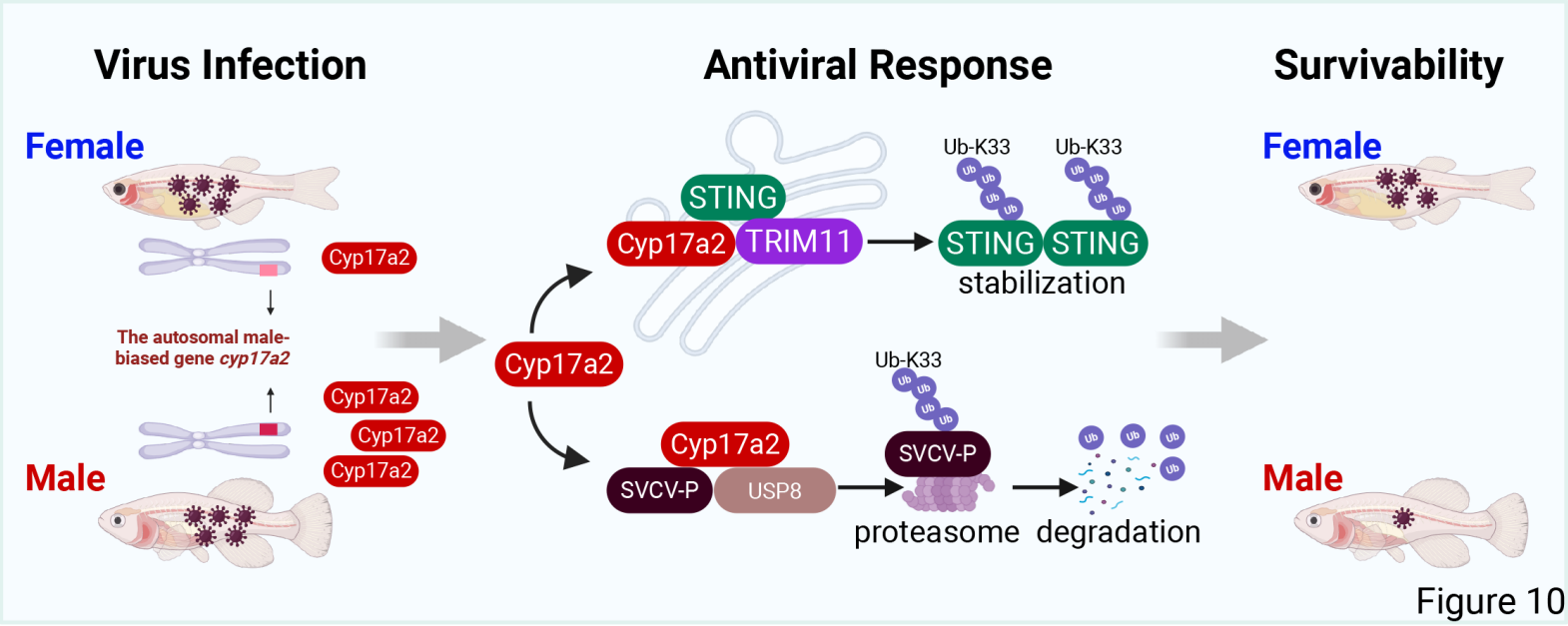
Virus Infection
Antiviral Response
Survivability
Female
Male
Cyp17a2
The autosomal male-biased gene cyp17a2
Cyp17a2
Cyp17a2
Cyp17a2
STING
Cyp17a2
TRIM11
Ub-K33
Ub-K33
STING
STING
stabilization
Ub-K33
Cyp17a2
SVCV-P
USP8
SVCV-P
proteasome
degradation
Female
Male

Figure 10

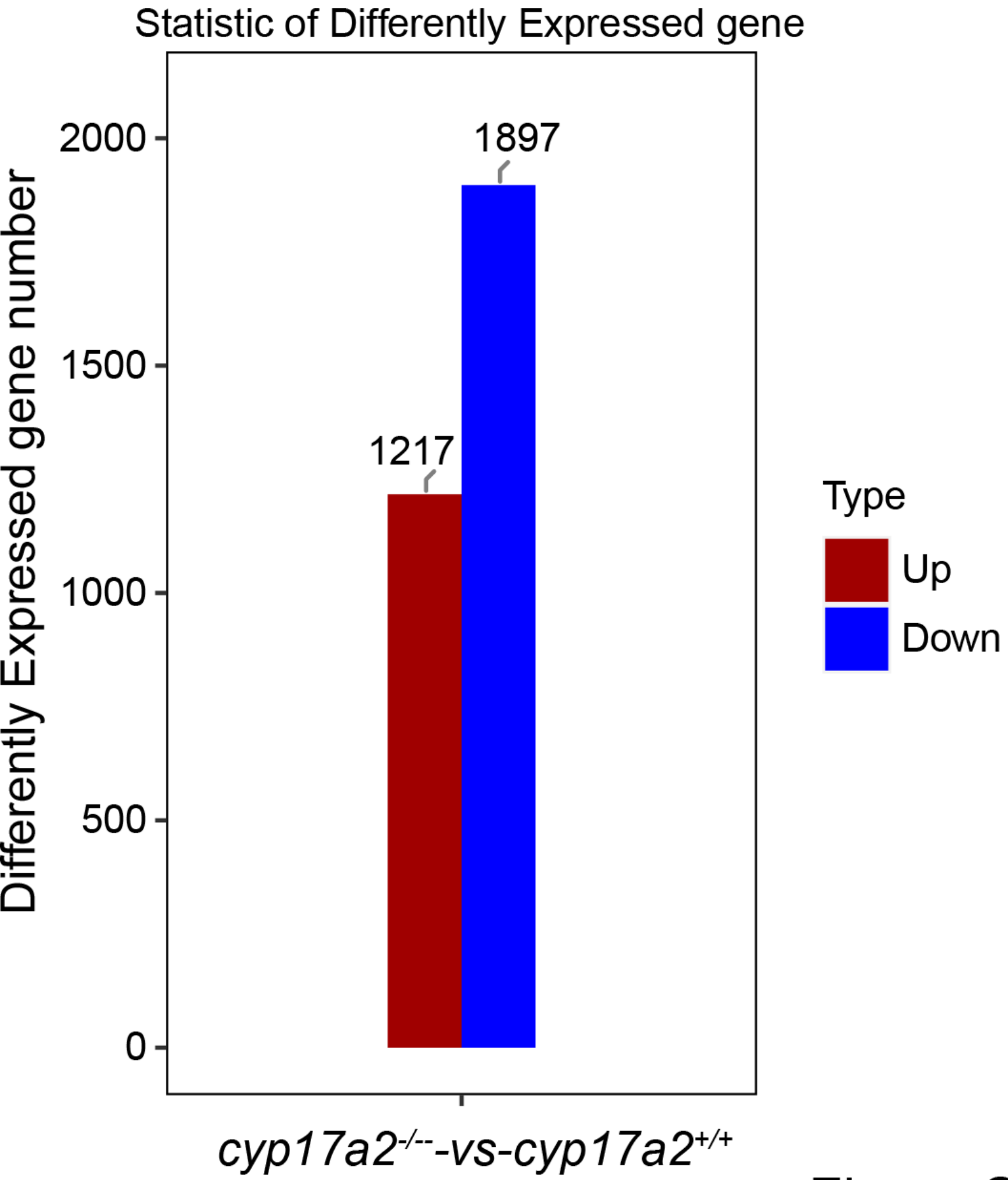
Statistic of Differently Expressed gene
Differently Expressed gene number
2000
1500
1000
500
0
1897
1217
Type
Up
Down
cyp17a2-/--vs-cyp17a2+/+

Figure S1

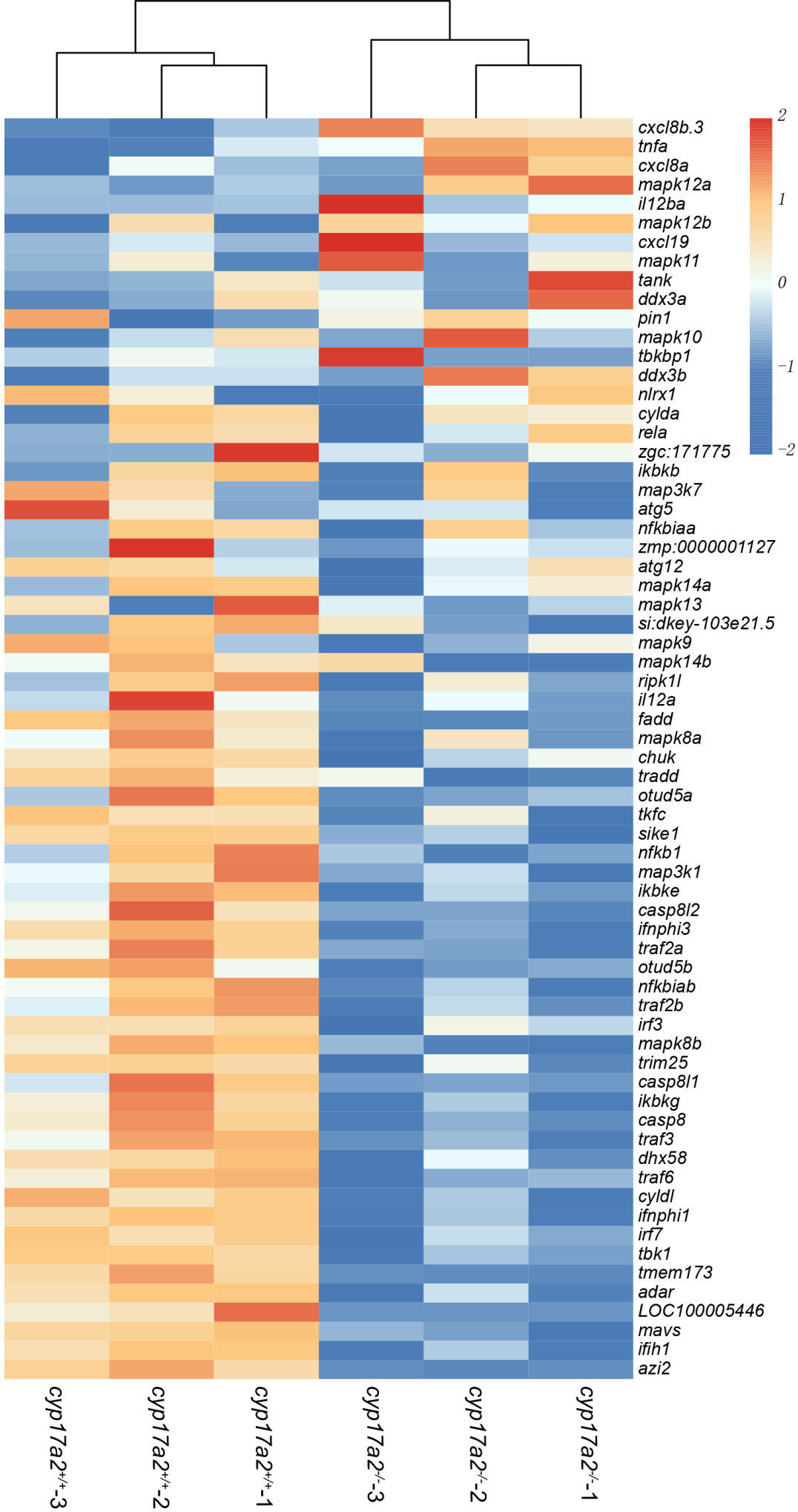
cxcl8b.3
tnfa
cxcl8a
mapk12a
il12ba
mapk12b
cxcl19
mapk11
tank
ddx3a
pin1
mapk10
tbkbp1
ddx3b
nlrx1
cylda
rela
zgc:171775
ikbkb
map3k7
atg5
nfkbiaa
zmp:0000001127
atg12
mapk14a
mapk13
si:dkey-103e21.5
mapk9
mapk14b
ripk1l
il12a
fadd
mapk8a
chuk
tradd
otud5a
tkfc
sike1
nfkb1
map3k1
ikbke
casp8l2
ifnphi3
traf2a
otud5b
nfkbiab
traf2b
irf3
mapk8b
trim25
casp8l1
ikbkg
casp8
traf3
dhx58
traf6
cyldl
ifnphi1
irf7
tbk1
tmem173
adar
LOC100005446
mavs
ifih1
azi2
2
1
0
−1
−2
cyp17a2+/+-3
cyp17a2+/+-2
cyp17a2+/+-1
cyp17a2-/--3
cyp17a2-/--2
cyp17a2-/--1

Figure S2